AMERICAN SOCIETY FOR MICROBIOLOGY | Journal of Virology®

STRUCTURE AND ASSEMBLY

# Analysis of Glycosylation and Disulfide Bonding of Wild-Type SARS-CoV-2 Spike Glycoprotein

**Shijian Zhang,[a] Eden P. Go,[b] Haitao Ding,[c] Saumya Anang,[a] John C. Kappes,[c,d] Heather Desaire,[b] Joseph G. Sodroski[a,e]**

[a]Department of Cancer Immunology and Virology, Dana-Farber Cancer Institute, Department of Microbiology, Harvard Medical School, Boston, Massachusetts, USA
[b]Department of Chemistry, University of Kansas, Lawrence, Kansas, USA
[c]Department of Medicine, University of Alabama at Birmingham, Birmingham, Alabama, USA
[d]Birmingham Veterans Affairs Medical Center, Research Service, Birmingham, Alabama, USA
[e]Department of Immunology and Infectious Diseases, Harvard T.H. Chan School of Public Health, Boston, Massachusetts, USA

Shijian Zhang and Eden P. Go contributed equally to this article. Authorship order was determined by mutual agreement.

**ABSTRACT** The SARS-CoV-2 coronavirus, the etiologic agent of COVID-19, uses its spike (S) glycoprotein anchored in the viral membrane to enter host cells. The S glycoprotein is the major target for neutralizing antibodies elicited by natural infection and by vaccines. Approximately 35% of the SARS-CoV-2 S glycoprotein consists of carbohydrate, which can influence virus infectivity and susceptibility to antibody inhibition. We found that virus-like particles produced by coexpression of SARS-CoV-2 S, M, E, and N proteins contained spike glycoproteins that were extensively modified by complex carbohydrates. We used a fucose-selective lectin to purify the Golgi-modified fraction of a wild-type SARS-CoV-2 S glycoprotein trimer and determined its glycosylation and disulfide bond profile. Compared with soluble or solubilized S glycoproteins modified to prevent proteolytic cleavage and to retain a prefusion conformation, more of the wild-type S glycoprotein N-linked glycans are processed to complex forms. Even Asn 234, a significant percentage of which is decorated by high-mannose glycans on other characterized S trimer preparations, is predominantly modified in the Golgi compartment by processed glycans. Three incompletely occupied sites of O-linked glycosylation were detected. Viruses pseudotyped with natural variants of the serine/threonine residues implicated in O-linked glycosylation were generally infectious and exhibited sensitivity to neutralization by soluble ACE2 and convalescent antisera comparable to that of the wild-type virus. Unlike other natural cysteine variants, a Cys15Phe (C15F) mutant retained partial, but unstable, infectivity. These findings enhance our understanding of the Golgi processing of the native SARS-CoV-2 S glycoprotein carbohydrates and could assist the design of interventions.

**IMPORTANCE** The SARS-CoV-2 coronavirus, which causes COVID-19, uses its spike glycoprotein to enter host cells. The viral spike glycoprotein is the main target of host neutralizing antibodies that help to control SARS-CoV-2 infection and are important for the protection provided by vaccines. The SARS-CoV-2 spike glycoprotein consists of a trimer of two subunits covered with a coat of carbohydrates (sugars). Here, we describe the disulfide bonds that assist the SARS-CoV-2 spike glycoprotein to assume the correct shape and the composition of the sugar moieties on the glycoprotein surface. We also evaluate the consequences of natural virus variation in O-linked sugar addition and in the cysteine residues involved in disulfide bond formation. This information can expedite the improvement of vaccines and therapies for COVID-19.

**KEYWORDS** COVID-19, SARS-CoV-2, coronavirus, viral protein, spike glycoprotein, glycosylation, disulfide, Golgi, virus entry, membrane protein

**Editor** Tom Gallagher, Loyola University Chicago



Address correspondence to Joseph G. Sodroski, joseph_sodroski@dfci.harvard.edu.

The authors declare no conflict of interest.

**Received** 17 September 2021
**Accepted** 12 November 2021
**Accepted manuscript posted online** 24 November 2021
**Published** 9 February 2022

The recently emerged severe acute respiratory syndrome coronavirus 2 (SARS-CoV-2) is responsible for the ongoing pandemic of coronavirus disease 2019 (COVID-19), a respiratory disease with an estimated 2 to 5% mortality (1–7). The SARS-CoV-2 spike (S) glycoprotein mediates the entry of the virus into the host cell and influences tissue tropism and pathogenesis (8–13). The S glycoprotein trimer in the viral membrane is the target for neutralizing antibodies, which are important for vaccine-induced protection against infection (9, 11, 12, 14–18). Monoclonal neutralizing antibodies directed against the S glycoprotein are being evaluated as treatments for SARS-CoV-2-infected individuals (14, 15, 19–26). In the virus-producing cell, the S glycoprotein is synthesized in the endoplasmic reticulum, where it assembles into trimers and is initially modified by high-mannose glycans (27, 28). Each of the three SARS-CoV-2 S glycoprotein protomers possesses 22 canonical sequons for N-linked glycosylation (11, 29–35). Coronavirus virions bud into the endoplasmic reticulum-Golgi intermediate compartment (ERGIC), and S glycoprotein trimers on the surface of these virus particles are thought to be processed further during trafficking through the Golgi complex (28, 36–39). In the Golgi complex, some of the glycans on the S glycoprotein are modified to complex carbohydrates; in addition, the trimeric S glycoprotein is cleaved by furin-related proteases into S1 and S2 glycoproteins, which associate noncovalently in the virus spike (26–35). During virus entry, the S1 subunit binds the receptor angiotensin-converting enzyme 2 (ACE2) (9, 11–13, 40–42). The S2 subunit is further processed by host proteases and undergoes extensive conformational changes to mediate the fusion of the viral and target cell membranes (42–46). Following the insertion of the S2 fusion peptide into the host cell membrane, the interaction of two helical heptad repeat regions (HR1 and HR2) on the S2 subunit brings the viral and cell membranes into proximity (43).

The SARS-CoV-2 S glycoprotein trimer is modified by glycosylation, which in other coronaviruses has been suggested to modulate accessibility to neutralizing antibodies as well as host proteases involved in S processing (11, 13, 29–31, 47, 48). Glycans camouflage S glycoprotein peptide epitopes, shielding them from potentially neutralizing antibodies. Glycans can also contribute to epitopes for antibody recognition; for example, the s309 neutralizing antibody interacts with the glycan on Asn 343 of the SARS-CoV-2 S glycoprotein (49).

Virus entry inhibitors and therapeutic or prophylactic neutralizing antibodies must recognize the mature SARS-CoV-2 spike with its natural glycan coat, as it exists on the viral membrane. The glycosylation of the SARS-CoV-2 spike has been studied using soluble or detergent-solubilized versions of the uncleaved S glycoprotein trimer, modified to retain a pretriggered conformation (29, 32–35, 50). Fewer studies of the glycosylation of S glycoproteins on SARS-CoV-2 virion preparations have been conducted (51, 52). Experience with human immunodeficiency virus (HIV-1) indicates that native, membrane-anchored viral envelope glycoproteins can exhibit glycosylation profiles that differ from those of soluble glycoprotein trimers (53–57). Here, we elucidate the glycosylation and disulfide bonding profile of a wild-type SARS-CoV-2 S glycoprotein trimer and evaluate the importance of naturally occurring variation in O-linked glycans and disulfide bonds. This information enhances our understanding of the complete, functional SARS-CoV-2 S glycoproteins and could assist the development and improvement of efficacious therapies, including monoclonal antibodies and vaccines.

## RESULTS

**SARS-CoV-2 S glycoproteins in cell lysates and VLPs.** We evaluated the wild-type SARS-CoV-2 S glycoprotein expressed alone or in combination with the viral membrane (M), envelope (E), and nucleocapsid (N) proteins, which direct the formation of virus-like particles (VLPs) (58, 59). In the absence of M, E, and N proteins, low levels of the S glycoprotein, presumably in extracellular vesicles, were detected in particles prepared by centrifugation of the supernatants of transiently expressing 293T cells (Fig. 1A to C). Coexpression of the M, E, and N proteins, particularly in combination, resulted in an increase in the level of S glycoprotein in the supernatant pellets. Both uncleaved S and cleaved (S1 and S2) glycoproteins were detected in the particles prepared from the cell supernatants (Fig. 1A and B). Two

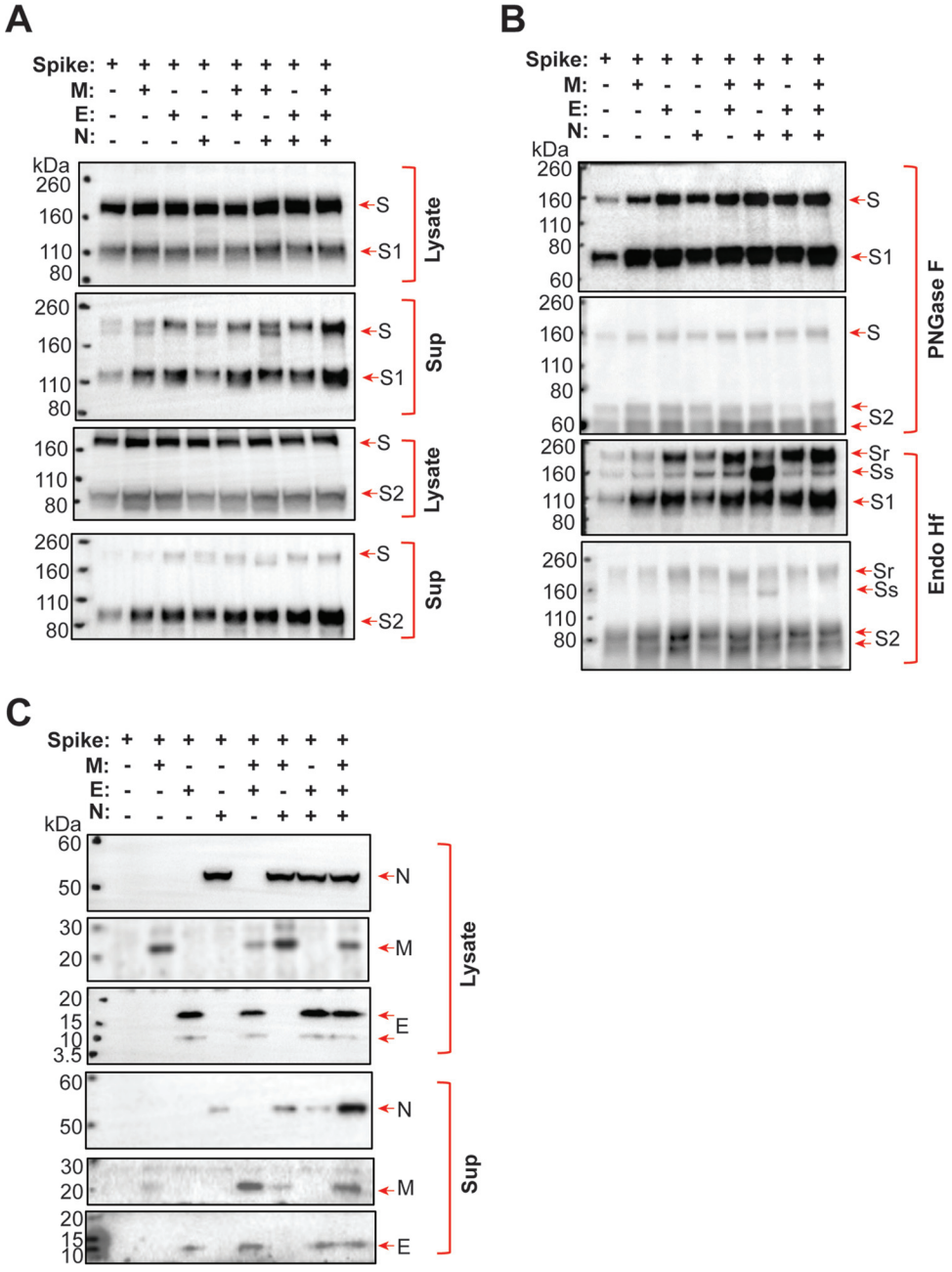


**FIG 1** Effect of coexpression of SARS-CoV-2 M, E, and N proteins on S glycosylation. (A to C) 293T cells were transfected with plasmids expressing the indicated SARS-CoV-2 proteins (S, spike glycoprotein; M, membrane protein; E, envelope protein; N, nucleocapsid protein). Two days after transfection, cells were lysed and particles were prepared by centrifugation of cell supernatants. (A) Cell lysates and supernatant pellets (Sup) were Western blotted with anti-S1 antibody (upper two panels) and anti-S2 antibody (lower two panels). (B) Supernatant pellets were treated with either PNGase F or Endo Hf and then Western blotted with anti-S1 or anti-S2 antibodies. Endo Hf-resistant and Endo Hf-sensitive forms of the S glycoprotein are indicated by Sr and Ss, respectively. (C) Cell lysates and supernatant pellets (Sup) were Western blotted with antibodies against the N, M, and E proteins. The results shown are typical of those obtained in three independent experiments.

forms of the uncleaved S glycoprotein were detected in the pelleted particles: (i) a faster-migrating form modified by endoglycosidase Hf (Endo Hf)-sensitive (high-mannose and/or hybrid) glycans and (ii) a more slowly migrating form modified by Endo Hf-resistant (complex) glycans (Fig. 1B). Coexpression of the E protein resulted in an increase in the ratio of complex to high-mannose glycans in the uncleaved S glycoprotein in the pelleted particles. Expression of the M, N, and S proteins without the E protein produced VLPs in which the

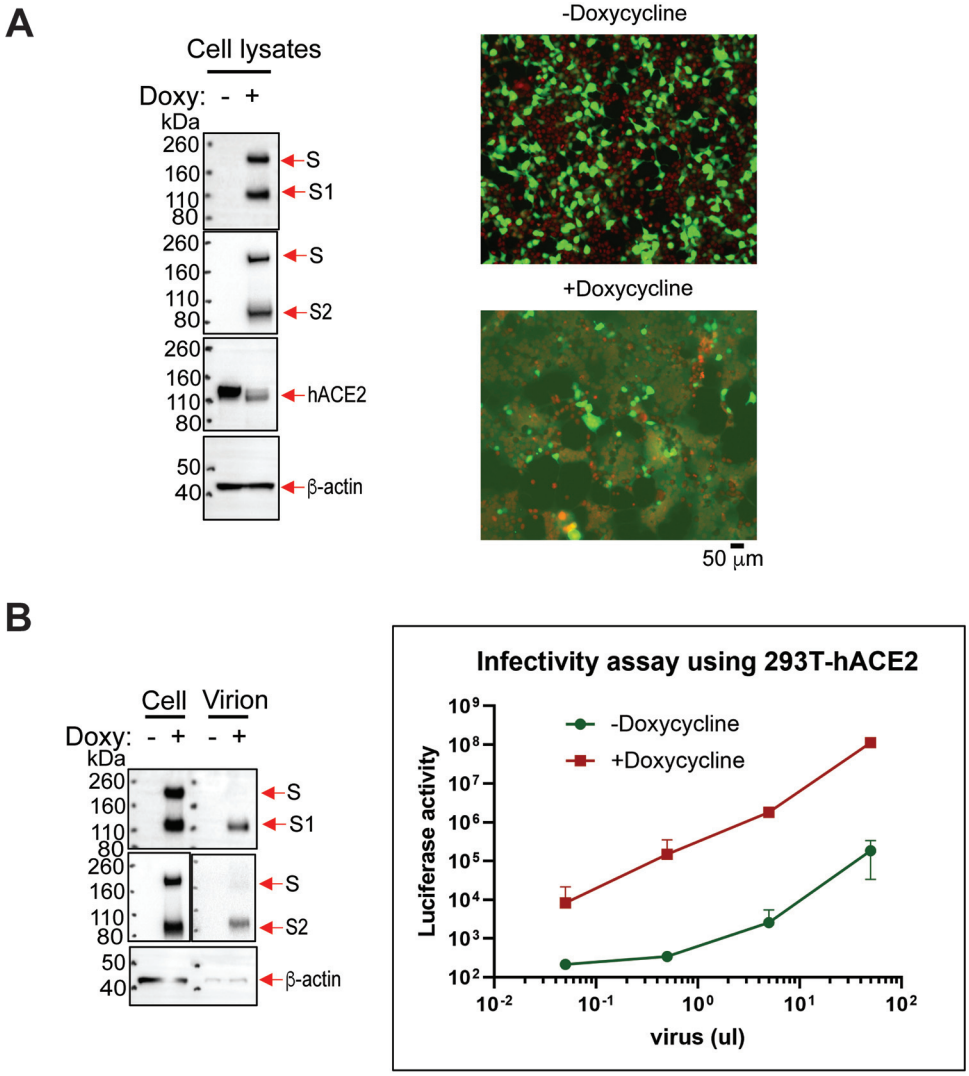


**FIG 2** Inducible expression of a functional SARS-CoV-2 S glycoprotein. (A) 293T-S cells were transfected with plasmids expressing eGFP and human ACE2 (hACE2) and then incubated in medium with or without 1 $\mu$g/ml doxycycline (Doxy). The next day, the cells were stained with NIR694 nuclear dye and imaged with a fluorescence microscope (right). In parallel, cell lysates were Western blotted with a mouse antibody against S1, a rabbit antibody against S2, a goat antibody against hACE2 and a mouse antibody against $\beta$-actin (left). The results shown are representative of those obtained in three independent experiments. Scale bar, 50 $\mu$m. (B) 293T-S cells were cultured for 24 h in medium with 1 $\mu$g/ml doxycycline (Doxy) or in control medium. The cells were then infected with a G glycoprotein-pseudotyped VSV$\Delta$G virus encoding luciferase. One day later, virus particles were harvested from precleared cell supernatants and incubated with 293T-hACE2 cells. Luciferase activity was measured 1 day later (right). Cell lysates and viruses concentrated by a 110,000 $\times$ *g* centrifugation were Western blotted with a mouse antibody against S1, a rabbit antibody against S2, and an anti-$\beta$-actin antibody (left). The results shown are a representative example of those obtained in two independent experiments.

Endo Hf-sensitive form of the uncleaved S glycoprotein was particularly abundant. The vast majority of the cleaved S1 and S2 glycoproteins in the pelleted VLPs were resistant to Endo Hf digestion (Fig. 1B). Thus, in the presence of SARS-CoV-2 M, E, and N proteins, the uncleaved and cleaved S glycoproteins on VLPs are largely modified by complex carbohydrates.

**Expression and purification of the SARS-CoV-2 S glycoprotein.** To study the native SARS-CoV-2 S glycoprotein in greater detail, we established a stable 293T cell line (293T-S) that expresses the wild-type SARS-CoV-2 S glycoprotein under the control of a tetracycline-inducible promoter (28). To facilitate purification, a carboxy-terminal 2$\times$Strep affinity tag was added to the S glycoprotein, which was otherwise wild type in sequence (28). Treatment of the 293T-S cells with doxycycline resulted in the expression of the S glycoprotein, which was cleaved into the S1 exterior and S2 transmembrane glycoproteins (Fig. 2A, left).

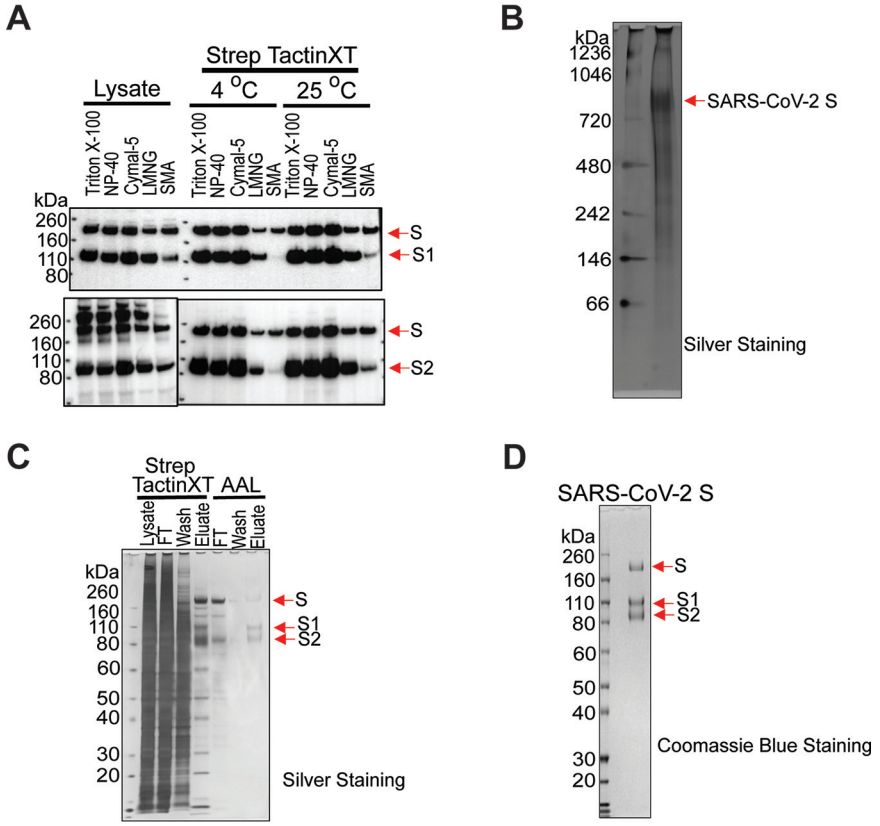


**FIG 3** Purification of the SARS-CoV-2 S glycoproteins. (A) 293T-S cells express the SARS-CoV-2 spike (S) glycoprotein in the absence of other viral proteins. 293T-S cells induced with doxycycline for 2 days were lysed in buffers containing the indicated detergents or styrene-maleic acid (SMA) copolymers. The cell lysates were either directly Western blotted (lysate) or used for S glycoprotein purification by Strep-Tactin XT at the indicated temperature. The purified S glycoproteins were Western blotted with rabbit antibodies against S1 (upper) and S2 (lower). (B) Purified S glycoproteins solubilized in SMA were analyzed on a blue native gel, which was stained with silver. (C) A lysate of 293T-S cells in a buffer containing Cymal-5 was purified by Strep-Tactin XT, followed by purification on *Aleuria aurantia* lectin (AAL)-agarose resin. The samples at various stages of purification were analyzed by SDS-PAGE and silver staining. FT, flowthrough fraction. (D) The purified S glycoproteins in a buffer containing Cymal-5 were analyzed by SDS-PAGE and Coomassie blue staining. Purification of the S glycoproteins was repeated more than four times, with comparable results.

The expressed S glycoproteins mediated the formation of syncytia when human ACE2 (hACE2) was transiently coexpressed in the 293T-S cells (Fig. 2A, right). The expressed S glycoproteins were incorporated into a vesicular stomatitis virus (VSV) vector (Fig. 2B, left). Nearly all of the S glycoproteins incorporated into VSV pseudotypes were cleaved. The VSV vector pseudotyped with the S glycoproteins was able to infect cells expressing human ACE2 (Fig. 2B, right).

For purification of the SARS-CoV-2 S glycoprotein, we evaluated several detergents as well as styrene-maleic acid (SMA) copolymers for their ability to extract the S glycoproteins from 293T-S membranes (60–65). NP-40, Triton X-100, and Cymal-5 solubilized the S glycoproteins more efficiently than lauryl maltose neopentyl glycol (LMNG) or SMA (Fig. 3A). The SMA-solubilized S glycoproteins migrated on a blue native gel more slowly than expected for trimers (Fig. 3B); membrane protein complexes in detergent or SMA often migrate more slowly than expected in blue native gels. Strep-Tactin purification of the cleaved S1/S2 complexes as well as the uncleaved S glycoproteins in Cymal-5 solutions was slightly more efficient than in the other detergents; therefore, we used Cymal-5 to extract the S glycoproteins for purification.

Both uncleaved and cleaved SARS-CoV-2 S glycoproteins are incorporated into VLPs formed as a result of expression of the SARS-CoV-2 M, E, and N proteins (59) (Fig. 1). Due to the relatively low yield of S glycoproteins from such VLPs, we purified quantities

of S glycoproteins adequate for mass spectrometric analysis from expressing cells. The S glycoproteins in VLPs are extensively modified by complex carbohydrates, indicating passage through the Golgi compartment. Therefore, we enriched the Golgi-modified, mature S glycoproteins by sequentially using Strep-Tactin and *Aleuria aurantia* lectin (AAL) to purify the S glycoproteins from the membranes of 293T-S cells (Fig. 3C). AAL recognizes fucose, which is added to a subset of complex glycans in the Golgi apparatus (66–69). The purified S glycoproteins consisted of approximately 25% uncleaved and 75% cleaved (S1 and S2) glycoproteins (Fig. 3D).

The unliganded SARS-CoV-2 S glycoproteins on VLPs are dynamic and spontaneously sample conformations in which all three S1 receptor-binding domains (RBDs) are down, one or two of the RBDs are up, or all three RBDs are up (70). ACE2 binding drives the S glycoprotein trimer from a closed conformation (with all three RBDs down) to more open conformations in which the RBDs are up (11, 13, 40, 50, 51, 71–79). We evaluated the ability of monoclonal antibodies (MAbs) that recognize specific conformations of the S glycoprotein trimer to precipitate the S glycoproteins in different contexts. MAb 2–4 recognizes closed spikes with all three RBDs in the down position (25). MAb 4–8 recognizes the N-terminal domain of the S glycoprotein; MAb 4–8 can recognize the closed spike but can also bind trimers in which one RBD is in the up position (25, 80). MAb 2–43 recognizes a quaternary epitope consisting of an RBD from one protomer and the glycan at Asn 343 on the RBD of an adjacent protomer (25, 81). MAb 2–43 binds the S glycoprotein trimer with RBDs in the down position, but antibody binding induces a more open conformation in which the RBDs move away from the trimer axis (81). CR3022 only recognizes more open S glycoproteins with RBDs in the up position (12, 82, 83). MAbs 2–4, 4–8, and 2–43 neutralize SARS-CoV-2, whereas CR3022 does not (12, 70, 82, 83). As shown in Fig. 4A, all four MAbs recognized the SARS-CoV-2 S glycoproteins on the surface of 293T-S cells. Of note, the 2–4, 2–43, and 4–8 neutralizing MAbs recognized both cleaved and uncleaved S glycoproteins, whereas the CR3022 nonneutralizing MAb recognized only the uncleaved S glycoprotein on the cell surface. The uncleaved S glycoprotein recognized by MAb CR3022 lacks complex glycans, whereas the uncleaved and cleaved S glycoproteins modified by complex carbohydrates were recognized by the 2–4, 2–43, and 4–8 MAbs. Thus, as seen previously (28), two forms of the uncleaved S glycoprotein can be detected on the surface of expressing cells, one modified by complex glycans and the other by high-mannose glycans. The CR3022, 2–4, 2–43, and 4–8 MAbs precipitated the S glycoproteins from cell lysates in a pattern similar to that seen for the cell-surface S glycoproteins (Fig. 4B). Next, we evaluated the ability of the MAbs to precipitate our purified S glycoprotein preparation. MAbs 2–4, 2–43, and 4–8 precipitated cleaved and uncleaved forms of the purified S glycoprotein preparation, whereas recognition of the purified S glycoproteins by the CR3022 MAb was at the background level seen for the control anti-HIV-1 MAb, 19b (Fig. 4C, left). Both cleaved and uncleaved forms of the purified S glycoproteins were precipitated by an sACE2-Fc fusion protein (84) (Fig. 4D). Soluble ACE2 decreased the binding of MAb 2–43 to the purified S glycoproteins, consistent with the expected disruption of its quaternary epitope by receptor-induced trimer opening (25, 81) (Fig. 4C, right). The precipitation of the purified S glycoproteins by MAb 2–4 was moderately decreased by sACE2, whereas that of MAb 4–8 was minimally affected. These results indicate that the closed conformation of the S glycoprotein trimer is represented in our preparation and that the purified S glycoproteins bind ACE2. Based on the negligible binding of the CR3022 MAb, the purified S glycoproteins do not predominantly sample open conformations in which the RBD is in an up position. Because the presence of residual fucose in the S glycoprotein preparation from AAL elution can generally decrease immunoprecipitation efficiency (data not shown), we do not rule out the possibility that a low percentage of the purified trimers sample open conformations.

To evaluate the representation of AAL-reactive S glycoproteins on SARS-CoV-2 VLPs, lysates prepared from VLPs were repeatedly precipitated with AAL-agarose resin or control protein A-agarose beads (Fig. 5). The vast majority of the S, S1, and S2 glycoproteins on SARS-CoV-2 VLPs could be recognized by AAL. These results are consistent with those shown in Fig. 1B and indicate that nearly all of the S glycoproteins on SARS-CoV-2 VLPs

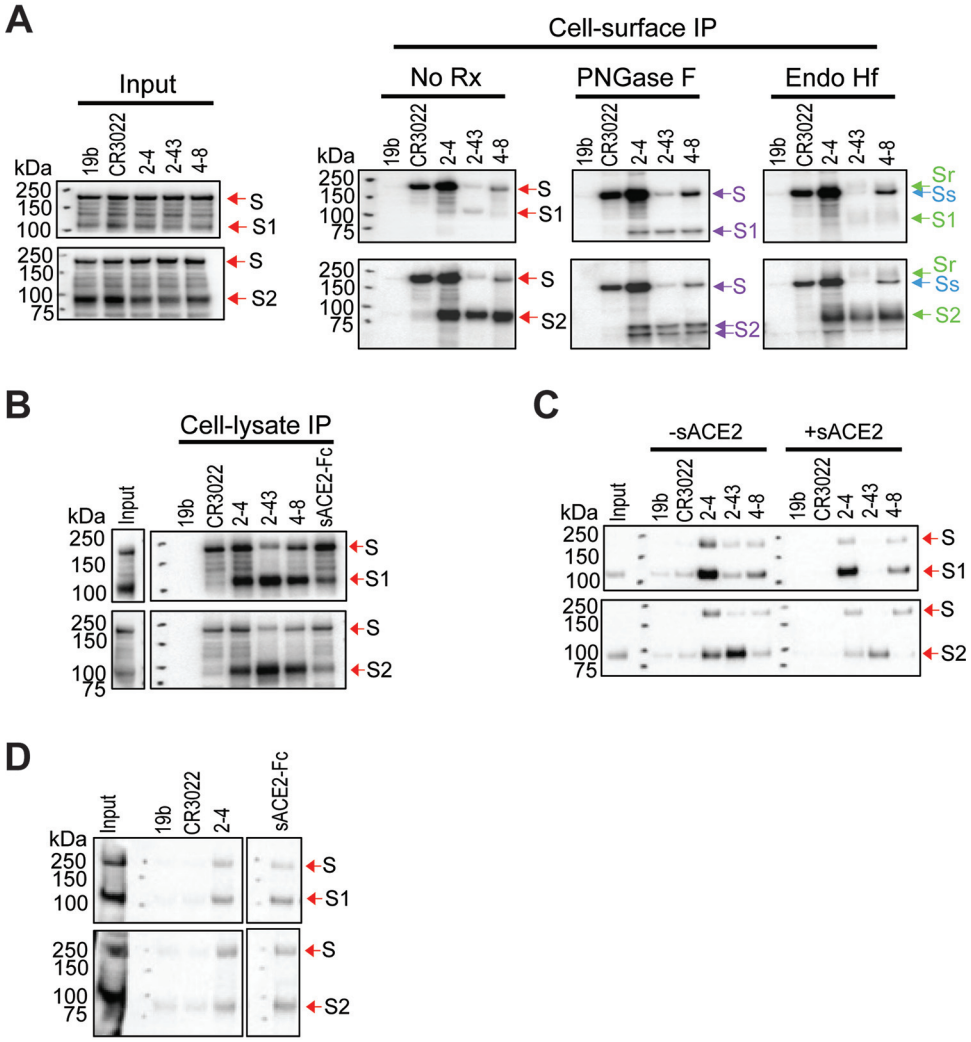


**FIG 4** MAb and sACE2 recognition of the S glycoproteins. (A) 293T-S cells induced with doxycycline for 2 days were incubated with the indicated MAbs to assess the ability of the antibody to recognize the cell-surface S glycoproteins. After washing, the cells were lysed. A fraction of the clarified cell lysates was analyzed by Western blotting, as described below (input samples, left). The remaining cell lysates were incubated with protein A-agarose beads. The precipitated proteins were treated with PNGase F or Endo Hf or left untreated (No Rx). The input cell lysates and cell surface immunoprecipitates (IP) were analyzed by Western blotting with mouse antibody against S1 (upper) and rabbit antibody against S2 (lower). Endo Hf-resistant (Sr) and Endo Hf-sensitive (Ss) forms of the uncleaved S glycoprotein are indicated. The 19b antibody against the HIV-1 gp120 glycoprotein serves as a negative control in these experiments. (B) Cell lysates were prepared from doxycycline-induced 293T-S cells and used for immunoprecipitation by the indicated MAbs. The input cell lysates and immunoprecipitates (IP) were analyzed by Western blotting with antibodies against S1 (upper) and S2 (lower). (C) The S glycoproteins, purified as described for Fig. 3, were precipitated by the indicated MAbs in the absence or presence of sACE2. (D) The purified S glycoproteins were precipitated by the indicated MAbs and by sACE2-Fc. The precipitated S glycoproteins in panels C and D were analyzed by Western blotting with antibodies against S1 (upper) and S2 (lower). The results shown in panels C and D are representative of those obtained in three independent experiments.

are modified by fucose-containing complex glycans. Therefore, AAL purification results in a representative sampling of relevant SARS-CoV-2 S glycoproteins.

**Disulfide and glycosylation analysis of the purified S glycoproteins.** The disulfide bond topology of the purified S glycoproteins was determined by identifying disulfide-linked peptides from the tryptic digests of the S glycoprotein preparation by mass spectrometry (MS) (Fig. 6 and 7). The S1 glycoprotein begins at an N-terminal glutamine (residue 14) that has undergone condensation to form pyroglutamine. The same N terminus has been observed for secreted, soluble forms of uncleaved SARS-CoV-2 S glycoprotein trimers (32). Ten disulfide bonds in S1 and five disulfide bonds in S2 were mapped (Fig. 7B). The cysteine

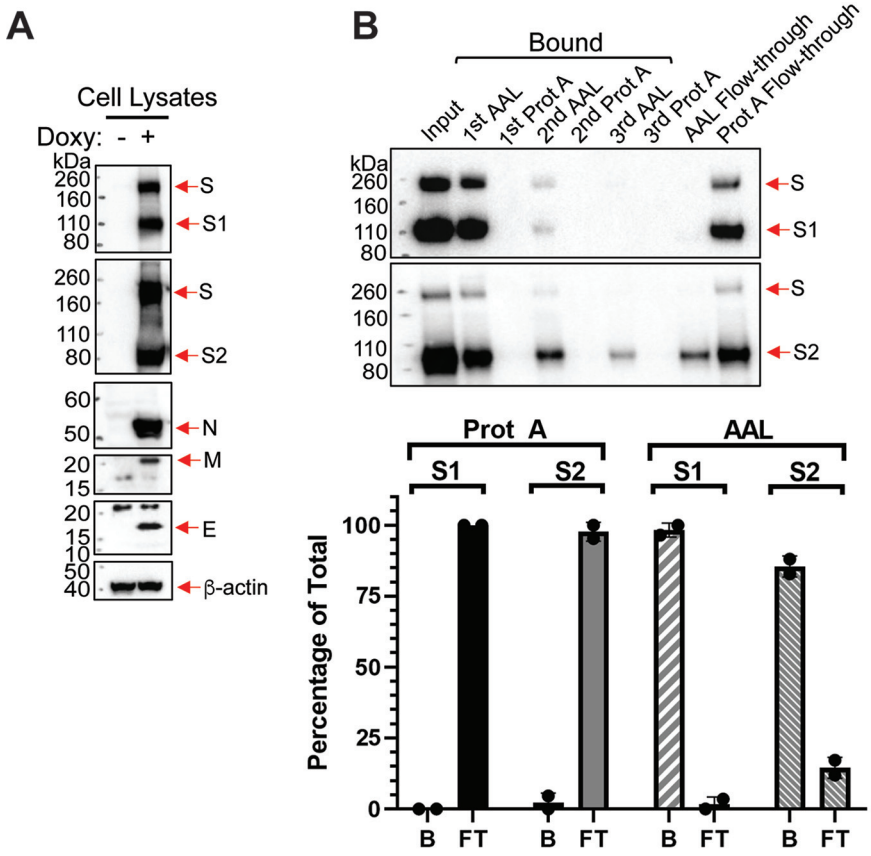


**FIG 5** AAL recognition of the S glycoproteins on SARS-CoV-2 VLPs. (A and B) 293T-S cells were transfected with plasmids expressing the SARS-CoV-2 M, E, and N proteins and incubated in medium with or without doxycycline (Doxy). (A) After 48 h, cell lysates were prepared and Western blotted with antibodies against the indicated proteins. (B) VLPs were prepared from the transfected cell supernatants. The VLPs were lysed and an aliquot was saved as the input. The remaining VLP lysate was divided equally and incubated with either AAL-agarose or protein A-agarose (Prot A) beads for three rounds. The S glycoproteins bound to the beads at each round and in the final flowthrough fractions were detected by Western blotting (upper two panels). In the lower panel, the total amounts of the S1 and S2 glycoproteins bound to the beads after all three successive precipitations (B) and in the final flowthrough (FT) fractions were quantitated and are shown as a percentage of the total (B plus FT) protein. The results shown are typical of those obtained in three independent experiments.

residues paired in the mapped disulfide bonds agree with those defined by structural analyses (11, 13, 71), consistent with proper folding of the purified S glycoproteins. We also observed an alternative disulfide bond between Cys 131 and Cys 136 in S1 (Fig. 6); in current S glycoprotein structures (11, 13, 71), these N-terminal domain cysteine residues are 12 to 15 Å apart and therefore are unable to form a disulfide bond without a change in conformation. Apparently, a fraction of the expressed S glycoproteins tolerates some plasticity in the N-terminal domain.

The glycan profile and glycosylation site occupancy of the 22 potential N-linked glycosylation sites were determined using an integrated glycopeptide-based MS approach described previously (53, 54, 85). With the exception of one site, Asn 1074, all of the N-linked glycosylation sites on this protein were fully occupied with glycans (Table 1). Asn 1074 was detected as partially occupied, although the unoccupied form is just one of over 50 different forms present at this site.

A pictorial description of the glycosylation profile of this protein is shown in Fig. 8. In sum, 826 unique N-linked glycopeptides were detected, along with 17 O-linked glycopeptides (see Table S1 in the supplemental material). This glycosylation coverage is more in-depth than early reports, where the number of unique glycoforms detected was more typically in the 100 to 200 range (29, 32, 34). Furthermore, this analysis provides the first report of O-linked glycosylation at 7 glycosylation sites: S659, S673, T676, S680, T696, T1160, and S1170.

| Canonical Disulfide Bonds in S1 | | | | |
|---|---|---|---|---|
| **Disulfide-Linked Peptides** | **CS** | **Theoretical m/z** | **Experimental m/z** | **Mass Error (ppm)** |
| Pyro-QC15VD17L<br>C136NDPF | 2+ | 576.7205 | 576.7203 | 0.3 |
| VC131EF<br>SSAND165C166TF | 2+<br>3+ | 669.7525<br>446.8374 | 669.7523<br>446.8371 | 0.3<br>1 |
| YNED282GTITDAVDC292ALDPLSETK<br>C301TLK | 2+<br>3+<br>4+ | 1416.1518<br>944.4370<br>708.5795 | 1416.1507<br>944.4364<br>708.5802 | 1<br>1<br>1 |
| FPD331ITNLC336PFGEVFD343ATR<br>ISNC361VADYSVLYNSASFSTFK | 3+<br>4+<br>5+ | 1452.3485<br>1089.5132<br>871.8120 | 1452.3494<br>1089.5133<br>871.8117 | 1<br>0.1<br>0.4 |
| C379YGVSPTK<br>LPDDFTGC432VIAWNSNNLDSK | 2+<br>3+<br>4+ | 1530.7076<br>1020.8075<br>765.8574 | 1530.7064<br>1020.8071<br>765.8571 | 1<br>0.4<br>0.4 |
| LNDLC391FTNVYADSFVIR<br>VVVLSFELLHAPATVC525GPK | 3+<br>4+<br>5+ | 1323.0214<br>992.5179<br>794.2158 | 1332.0214<br>992.5179<br>794.2166 | 0<br>0<br>1 |
| DISTEIYQAGSTPC480NGVEGFNC488YFPLQSYG-FQPTNGVGYQPYR | 3+<br>4+<br>5+ | 1589.3796<br>1192.2865<br>954.0306 | 1589.3718<br>1192.2851<br>954.0294 | 1<br>1<br>1 |
| C538VNF<br>DITPC590SF | 2+<br>3+ | 631.2651<br>421.1791 | 631.2645<br>421.1786 | 1<br>1 |
| QDVDC617TEVPVAIH<br>AGC649L | 2+<br>3+<br>4+ | 893.4110<br>595.9431<br>447.2091 | 893.4107<br>595.9428<br>447.2090 | 0.3<br>0.4<br>0.3 |
| EC662DIPIGAGIC671ASY | 1+<br>2+ | 1409.6077<br>705.3075 | 1409.6068<br>705.3066 | 1<br>1 |
| **Alternative Disulfide Bond in S1** | | | | |
| **Disulfide-Linked Peptides** | **CS** | **Theoretical m/z** | **Experimental m/z** | **Mass Error (ppm)** |
| VC131EFQFC136NDPFLGVYYHK | 2+<br>3+<br>4+ | 1103.9899<br>736.3290<br>552.4986 | 1103.9915<br>736.3296<br>552.4985 | 1<br>1<br>0.2 |

**FIG 6** Disulfide bond topology of the S1 subunit of the purified S glycoproteins. MS analysis of the purified S1 glycoproteins identified 10 canonical disulfide bonds between the cysteine residues highlighted in red (upper). Glycosylated asparagine residues converted to aspartic acid residues by PNGase F treatment are highlighted in blue. The MS analysis also identified one alternative disulfide bond in the S1 glycoprotein (lower).

As can be seen in Fig. 8, processed glycoforms predominated at each N-linked glycosylation site, and, as shown in Fig. 9A, these complex forms were highly, but not exclusively, fucosylated. Additionally, even though each glycosylation site was heavily processed in the Golgi compartment, the sialic acid content varied across the protein sequence. Some sites, like N61 and N343, had no sialylated glycoforms detected, while most of the sites in the S2 protein, particularly those nearest the C terminus, were abundantly sialylated. Finally, as shown in Fig. 9B, a number of O-linked glycoforms were detected.

The vast majority of the N-linked glycans on the Golgi-enriched, wild-type SARS-CoV-2 S glycoproteins expressed in 293T cells were processed to complex glycans. In Fig. 10, we compare our results with available glycosylation analyses of soluble or solubilized SARS-CoV-2 S glycoproteins. These include wild-type S glycoproteins purified from SARS-CoV-2 virions as well as soluble and full-length S glycoprotein trimers modified to inhibit furin cleavage and to stabilize a prefusion conformation (29, 32, 33, 35, 50–52, 86, 87). The glycans on individually expressed SARS-CoV-2 S1 and S2 glycoproteins have also been analyzed (34). All studies agree

**A**

| Disulfide-Linked Peptides | CS | Theoretical m/z | Experimental m/z | Mass Error (ppm) |
|---|---|---|---|---|
| TSVDC738TMYIC743GDSTEC749SNLLLQYGSFC760TQLNR | 2+ | 1718.2587 | 1781.2590 | 0.2 |
| | 3+ | 1187.8415 | 1187.8420 | 0.4 |
| | 4+ | 891.1330 | 891.1333 | 0.4 |
| QYGDC840LGDIAAR<br>DLIC851AQK | 2+ | 1034.9933 | 1034.9937 | 0.4 |
| | 3+ | 690.3313 | 690.3318 | 1 |
| | 4+ | 518.0002 | 518.0004 | 0.3 |
| MSEC1032VLGQSK<br>VDFC1043GK | 2+ | 873.8967 | 873.8970 | 0.3 |
| | 3+ | 582.9336 | 582.9337 | 0.2 |
| | 4+ | 437.4520 | 437.4520 | 0 |
| TTAPAIC1082HDGK<br>VSGNC1126DVVIGIVD1134NTVY | 2+ | 1439.1915 | 1439.1914 | 0 |
| | 3+ | 959.7967 | 959.7961 | 0.4 |
| | 4+ | 720.0994 | 720.0992 | 0.2 |

**B**

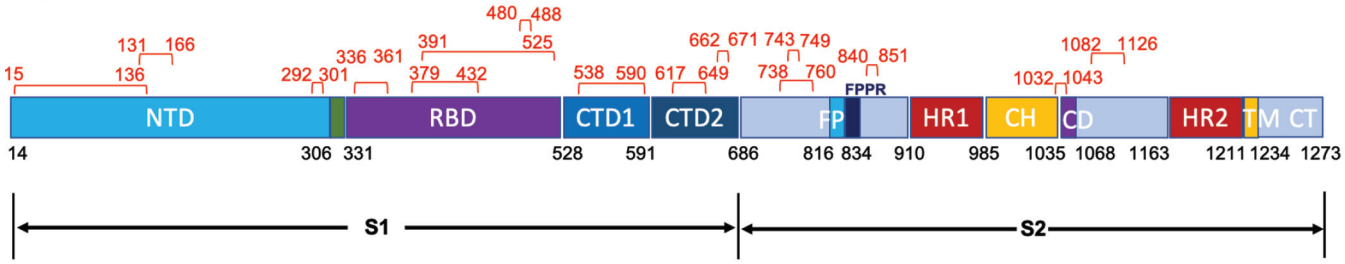


**FIG 7** Disulfide bond topology of the purified S glycoproteins. (A) MS analysis of the purified S2 glycoproteins identified 5 canonical disulfide bonds. Cysteine residues participating in the disulfide bonds are highlighted in red. The glycosylated asparagine residue converted to an aspartic acid residue by PNGase F treatment is highlighted in blue. (B) The canonical disulfide bonds identified by MS are shown in red above a schematic representation of the SARS-CoV-2 S glycoprotein. The S glycoprotein regions include the N-terminal domain (NTD), receptor-binding domain (RBD), C-terminal domains (CTD1 and CTD2), fusion peptide (FP), fusion peptide-proximal region (FPPR), heptad repeat regions (HR1 and HR2), central helical region (CH), the connector domain (CD), transmembrane region (TM), and cytoplasmic tail.

that complex carbohydrates are found on most of the N-linked glycan sites on SARS-CoV-2 S glycoprotein trimers as well as on recombinant soluble S1 and S2 glycoproteins. However, the extent of N-linked glycan processing in our study is greater than that seen for either soluble S glycoprotein trimers or for modified (cleavage-defective, proline-substituted) S glycoprotein variants (29, 32, 33, 35, 50). The glycosylation profile of our Golgi-enriched S glycoprotein preparation most closely resembles that of S glycoproteins purified from SARS-CoV-2 virions propagated in Vero cells (51) (Fig. 10). However, in our S glycoprotein preparation, Asn 234 in the S1 N-terminal domain is mostly processed, whereas high-mannose glycans are retained at this site in the other characterized S glycoprotein variants. While different laboratories measure the glycoform percentages differently and these methodological differences can explain some of the variability seen in Fig. 10, another important issue to note is the significant increase in the number of processed glycoforms reported in this study. In the S glycoprotein from Vero cells, only four processed forms were detected (51); in this study, 35 forms are identified. The supplemental material contains 10 examples of annotated tandem mass spectrometry (MS/MS) data with newly detected and complex glycoforms from the Asn 234 site (Fig. S1).

The highest composition of high-mannose glycans in our study mapped to a glycopeptide containing two potential N-linked glycosylation sites at Asn 709 and Asn 717. Although we cannot precisely assign a glycan composition at either site, our result is consistent with observations on soluble/modified S glycoproteins suggesting that one or both of these sites is occupied by a significant percentage of high-mannose glycans (29, 32, 33). The location of these glycans in a heavily glycosylated region near the

**TABLE 1** Glycosylation site occupancy[a]

| Glycosylation | No. of PNG or O-linked sites | Occupancy |
|---|---|---|
| N-linked | | |
| Pyro_QCV**N**$^{17}$LTTR | 1 | 1 |
| FS**N**$^{61}$VTWF | 1 | 1 |
| HAIHVSGT**N**$^{74}$GTK | 1 | 1 |
| TQSLLIVN**N**$^{122}$ATNVVIK/IVN**N**$^{122}$ATNVVIK | 1 | 1 |
| HK**N**$^{149}$NKSWMESEF/**N**$^{149}$NK | 1 | 1 |
| VYSSAN**N**$^{165}$CTFEYVSQPFLMDLEGK/SSAN**N**$^{165}$CTF | 1 | 1 |
| DLPQGFSALEPLVDLPIGI**N**$^{234}$ITR/SALEPLVDLPIGI**N**$^{234}$ITR | 1 | 1 |
| YNE**N**$^{282}$GTITDAVDCALDPLSETK | 1 | 1 |
| FP**N**$^{331}$ITNLCPF/FP**N**$^{331}$ITNL | 1 | 1 |
| GEVF**N**$^{343}$ATRF/**N**$^{343}$ATRF | 1 | 1 |
| GGVSVITPGT**N**$^{603}$TSNQVAVLY | 1 | 1 |
| QDV**N**$^{616}$CTEVPVAIHADQLTPTWR/QDV**N**$^{616}$CTEVPVAIHADQL | 1 | 1 |
| AGCLIGAEHV**N**$^{657}$NSYECDIPIGAGICASYQTQTNSPR/AGCLIGAEHV**N**$^{657}$NSY | 1 | 1 |
| SVASQSIIAYTMSLGAENSVAYS**N**$^{709}$NSIAIPT**N**$^{717}$FTISVTTEILPVSMTK/S**N**$^{709}$NSIAIPT**N**$^{717}$F | 2 | 2 |
| DFGGF**N**$^{801}$FSQILPDPSKPSK/TPPIKDFGGF**N**$^{801}$FSQILPDPSKPSK | 1 | 1 |
| GYHLMSFPQSAPHGVVFLHVTYVPAQEK**N**$^{1074}$FTTAPAICHDGK/**N**$^{1074}$FTTAPAICHDGK/VPAQEK**N**$^{1074}$F | 1 | 0 and 1 |
| EGVFVS**N**$^{1098}$GTHWFVTQR/VFVS**N**$^{1098}$GTHW | 1 | 1 |
| VSGNCDVVIGIV**N**$^{1134}$NTVY | 1 | 1 |
| **N**$^{1158}$HTSPDVDLGDISGI**N**$^{1173}$ASVVNIQK | 2 | 2 |
| NL**N**$^{1194}$ESLIDLQELGK | 1 | 1 |
| O-linked | | |
| VQP*T*$^{323}$E*S*$^{325}$IVR | 2 | 0 and 1 |
| AGCLIGAEHVNN*S*$^{659}$YECDIPIGAGICA*S*$^{673}$YQ*T*$^{676}$Q *T*$^{678}$N*S*$^{680}$PR | 5 | 0, 1, and 2 |
| *T*$^{696}$MSLGAENSVAY | 1 | 0 and 1 |
| NH*T*$^{1160}$SPDVDLGDI*S*$^{1170}$GINASVVNIQK | 2 | 0 and 1 |

[a]The sequences of the SARS-CoV-2 glycopeptides with N-linked glycosylation and O-linked glycosylation are shown, with the potential sites of glycosylation highlighted in boldface and italics, respectively. The occupancy at each potential N-linked glycosylation (PNG) or O-linked glycosylation site is indicated.

base of the S1 subunit may limit the access of glycosylation enzymes and predispose to the retention of high-mannose glycans (Fig. 11).

O-linked glycosylation of two S1 glycopeptides and two S2 glycopeptides was detected (Fig. 9B). Potential candidates for O-glycosylated residues include Thr 323, Ser 325, Ser 659, Ser 673, Thr 676, Thr 678, and Ser 680 in S1 and Thr 696, Thr 1160, and Ser 1170 in S2. O-linked glycosylation at Thr 323/Ser 325 was reported for soluble S glycoproteins and virion S glycoprotein trimers, but with low occupancy; in some cases, less than 1% of the residues were modified (32, 34, 35, 52). In this study, the occupancy rate for these two sites is also around 1% (Table 1). Thr 678 has also been reported to be O-glycosylated in soluble and virion S glycoproteins, with higher occupancy than that for Thr 323/Ser 325 (35, 52). In our study, the peptide containing Ser 659, Ser 673, Thr 676, Thr 678, and Ser 680 was found to be occupied by at least one O-linked glycan at a level of about 5%. MS/MS data for several examples of the novel O-linked glycoforms are provided in Fig. S1.

**SARS-CoV-2 S glycoprotein expression in a cell line with defective glycosylation.** GALE/GALK2 293T cells defective for O-linked glycosylation have been established (88). Both the wild-type SARS-CoV-2 S glycoprotein and the prevalent D614G variant S glycoprotein (28, 89–94) were expressed in 293T cells and in the GALE/GALK2 293T cells. Both the S1 and S2 glycoproteins of the wild-type and D614G SARS-CoV-2 strains migrated faster when expressed in the GALE/GALK2 293T cells compared with the migration of these glycoproteins expressed in 293T cells (Fig. 12A). Digestion of the glycoproteins with PNGase F revealed that the observed differences in S1 migration could be explained by differences in N-linked glycosylation. PNGase F digestion of the S2 glycoprotein resulted in 60- and 63-kDa products. The 60-kDa PNGase F-produced S2 proteins expressed in wild-type and GALE/GALK2 293T cells migrated similarly, ruling out a significant level of O-linked glycosylation. The 63-kDa PNGase F S2 product potentially is O-glycosylated, as it migrated faster when synthesized in the GALE/GALK2 293T cells. However, the 63-kDa product observed after PNGase F digestion was minimally affected by further treatment with O-glycosidase plus neuraminidase. Moreover, no significant difference in the migration of the untreated S1 and

Glycosylation Analysis of the SARS-CoV-2 S Glycoproteins

Summary:

| Glycosylation | Number | Detected | No. of Glycans |
|---|---|---|---|
| N-linked | 22 | 22 | 826* |
| O-linked | 3 previously reported ($T^{323}$,$S^{325}$,$T^{678}$) | 10 detected($T^{323}$,$S^{325}$,$S^{659}$,$S^{673}$,$T^{676}$, $T^{678}$,$S^{680}$,$T^{696}$,$T^{1160}$,$S^{1170}$) | 17 |

* Total N-linked glycans used in the bar graph

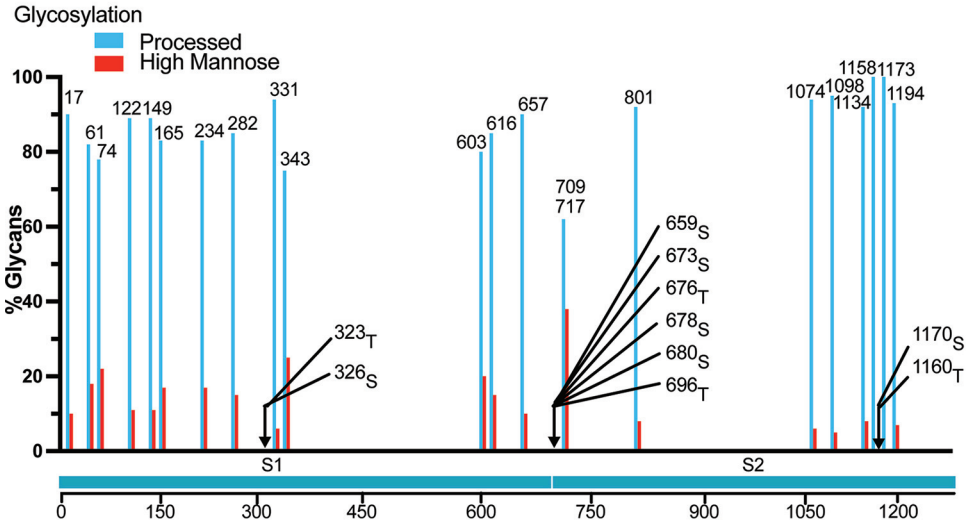


**FIG 8** Glycosylation profile of the purified S glycoproteins. MS analysis of the purified S glycoproteins identified 22 N-linked glycosylation sites as well as O-linked glycosylation sites, summarized in the upper panel. The glycan composition at each N-linked glycosylation site is shown in the lower panel. Serine and threonine residues contained in glycopeptides with O-linked carbohydrates are indicated by arrows.

S2 glycoproteins was observed after O-glycosidase plus neuraminidase treatment. We note that the core 1 O-linked glycans detected on the purified S glycoproteins should be digestible by O-glycosidase plus neuraminidase, as was shown on a control substrate, fetuin (Fig. 12B). Taken together, these results indicate that O-glycan occupancy is low on the SARS-CoV-2 S glycoproteins expressed in 293T cells. Variation in other posttranslational modifications, including N-linked glycosylation, apparently accounts for most of the observed differences in the migration of S1 and S2 glycoproteins expressed in wild-type and GALE/GALK2 293T cells. When the S glycoproteins produced in GALE/GALK2 293T cells were used to pseudotype vesicular stomatitis virus (VSV) vectors, the resulting viruses exhibited lower infectivity than viruses made with S glycoproteins produced in 293T cells (data not shown). These results suggest that differences in the posttranslational modifications of S glycoproteins produced in 293T and GALE/GALK2 293T cells influence S glycoprotein function. As only a fraction of the S glycoprotein is modified by O-linked glycans in 293T cells, differences in O-linked glycosylation are unlikely to explain the observed reduction in the infectivity of VSV(S) pseudotypes produced in GALE/GALK2 293T cells.

**Natural variants of SARS-CoV-2 S glycoproteins.** Rare natural variants of SARS-CoV-2 S glycoproteins exhibit substitutions at one of the cysteine residues, potentially compromising the formation of particular disulfide bonds (92, 93). We wished to assess the impact of these substitutions on S glycoprotein expression, processing, and function. The C15F change eliminates the Cys 15-Cys 136 disulfide bond in the S1 N-terminal domain. Despite this alteration, the C15F S glycoprotein was proteolytically processed nearly as efficiently as the wild-type S glycoprotein and exhibited wild-type association of the S1 and S2 subunits (Fig. 13 and 14). The infectivity of VSV vectors pseudotyped with the C15F S glycoproteins was approximately 31% of that of virus pseudotyped with the wild-type S glycoproteins (Fig. 14B). However, after freeze-thawing, the relative infectivity of the C15F mutant virus decreased dramatically (data not shown). Apparently, the Cys 15-Cys 136 disulfide bond is not absolutely essential for S glycoprotein function but may contribute to the stability of

**A**

***N-Linked Sites: 22 sites***

| Glycosylated Peptides (N-Linked) | Count | %HM | % Proc | %Fuc | % Sia |
|---|---|---|---|---|---|
| Pyro_QCVN17LTTR | 63 | 10 | 90 | 86 | 35 |
| FSN61VTWF | 28 | 18 | 82 | 48 | 0 |
| HAIHVSGTN74GTK | 27 | 22 | 78 | 91 | 33 |
| TQSLLIVNN122ATNVVIK/IVNN122ATNVVIK | 47 | 11 | 89 | 60 | 29 |
| HKN149NKSWMESEF/N149NK | 18 | 11 | 89 | 81 | 50 |
| VYSSANN165CTFEYVSQPFLMDLEGK/SSANN165CTF | 29 | 17 | 83 | 54 | 25 |
| DLPQGFSALEPLVDLPIGIN234ITR/SALEPLVDLPIGIN234ITR | 42 | 17 | 83 | 60 | 20 |
| YNEN282GTITDAVDCALDPLSETK | 47 | 15 | 85 | 58 | 12 |
| FPN331ITNLCPF/FPN331ITNL | 36 | 6 | 94 | 79 | 35 |
| GEVFN343ATRF/ N343ATRF | 20 | 25 | 75 | 73 | 0 |
| GGVSVITPGTN603TSNQVAVLY | 30 | 20 | 80 | 67 | 4 |
| QDVN616CTEVPVAIHADQLTPTWR/ QDVN616CTEVPVAIHADQL | 41 | 15 | 85 | 66 | 26 |
| AGCLIGAEHVN657NSYECDIPIGAGICASYQTQTNSPR/AGCLIGAEHVN657NSY | 20 | 10 | 90 | 100 | 39 |
| SVASQSIIAYTMSLGAENSVAYSN709NSIAIPTN717FTISVTTEILPVSMTK/SN709NSIAIPTN717F | 26 | 38 | 62 | 56 | 0 |
| DFGGFN801FSQILPDPSKPSK/TPPIKDFGGFN801FSQILPDPSKPSK | 67 | 8 | 92 | 53 | 37 |
| GYHLMSFPQSAPHGVVFLHVTYVPAQEKN1074FTTAPAICHDGK / N1074FTTAPAICHDGK / VPAQEKN1074F | 92 | 6 | 94 | 62 | 36 |
| EGVFVSN1098GTHWFVTQR/VFVSN1098GTHW | 92 | 5 | 95 | 49 | 56 |
| VSGNCDVVIGIVN1134NTVY | 66 | 8 | 92 | 87 | 48 |
| N1158HTSPDVDLGDISGIN1173ASVVNIQK | 5 | 0 | 100 | 100 | 80 |
| NLN1194ESLIDLQELGK | 30 | 7 | 93 | 93 | 75 |

**B**

***O-Linked Sites: 10 sites***

| Glycosylated Peptides (O-Linked) | Number of Glycans |
|---|---|
| VQPT323ES325IVR | 4 |
| AGCLIGAEHVN657NS659YECDIPIGAGICAS673YQT676Q T678NS680PR | 9 |
| T696MSLGAENSVAY | 1 |
| N1158HT1160SPDVDLGDIS1170GIN1173ASVVNIQK | 3 |

**FIG 9** SARS-CoV-2 S glycopeptides. (A) The sequences of the S glycopeptides with N-linked glycosylation are shown, with the modified asparagine residues highlighted in red. The percentage of glycans that are high-mannose (HM), processed (Proc) (complex plus hybrid), modified by fucose (Fuc), or sialylated (Sia) are indicated. The glycan percentages were derived from multiple, complementary LC-MS analyses; as described in Materials and Methods, the LC-MS results from different digestion conditions were combined to obtain a complete, aggregate profile. Each glycoform in the complete glycan profile was manually validated by HR-MS and MS/MS in at least one of the data sets that was acquired. (B) The sequences of S glycopeptides with O-linked glycosylation are shown, with the potentially modified serine and threonine residues highlighted in green. Asparagine residues in the glycopeptides that are modified by N-linked glycans are highlighted in red.

the functional spike. In contrast, the C301F and C379F changes, which eliminate the Cys 291-Cys 301 and Cys 379-Cys 432 disulfide bonds, respectively, located in the S1 N-terminal domain and receptor-binding domain, resulted in S glycoproteins that were not processed into S1 and S2 glycoproteins (Fig. 13 and 14). Viruses pseudotyped with the C301F and C379F S glycoproteins exhibited very low levels of infectivity (Fig. 14B). Thus, of these rare cysteine variants of the SARS-CoV-2 S glycoprotein, only one (C15F) allows partial, but unstable, infectivity.

To evaluate the potential O-linked glycosylation of the SARS-CoV-2 S glycoprotein, several of the threonine and serine residues implicated in our MS study were altered to residues found in natural SARS-CoV-2 variants (92, 93). The T323I, T676I, and S1170F mutants were processed nearly as efficiently as the wild-type S glycoprotein and exhibited

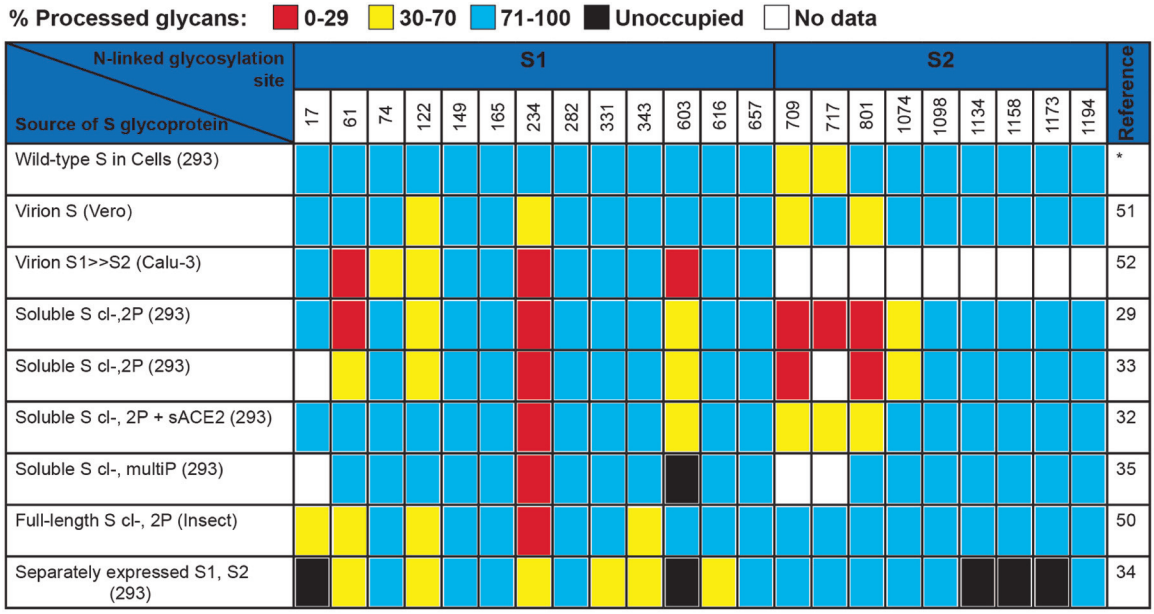


**FIG 10** Glycan composition of different SARS-CoV-2 S glycoprotein preparations. The glycan composition at each of the potential S glycoprotein N-linked glycosylation sites from this study (upper row) (asterisk) is compared with those defined for SARS-CoV-2 S glycoproteins from various sources. Some of the S glycoproteins have been produced in soluble forms with alterations of the furin cleavage site (cl-) and with proline substitutions (2P or multiP) to stabilize prefusion conformations.

good subunit association (Fig. 13A and 14A). The 63-kDa S2 glycoprotein band seen in PNGase F-treated lysates from 293T cells expressing the wild-type S glycoproteins was not evident in lysates from cells expressing the S1170F mutant (Fig. 13B and C). As the S1170F change does not alter a potential N-linked glycosylation site, it apparently affects other post-translational modifications; as discussed above, resistance of the 63-kDa PNGase F product to O-glycosidase appears to rule out modification by core 1 or core 3 O-glycans (Fig. 13C). The S676I and S1170F mutants supported the entry of VSV pseudotypes as efficiently as the

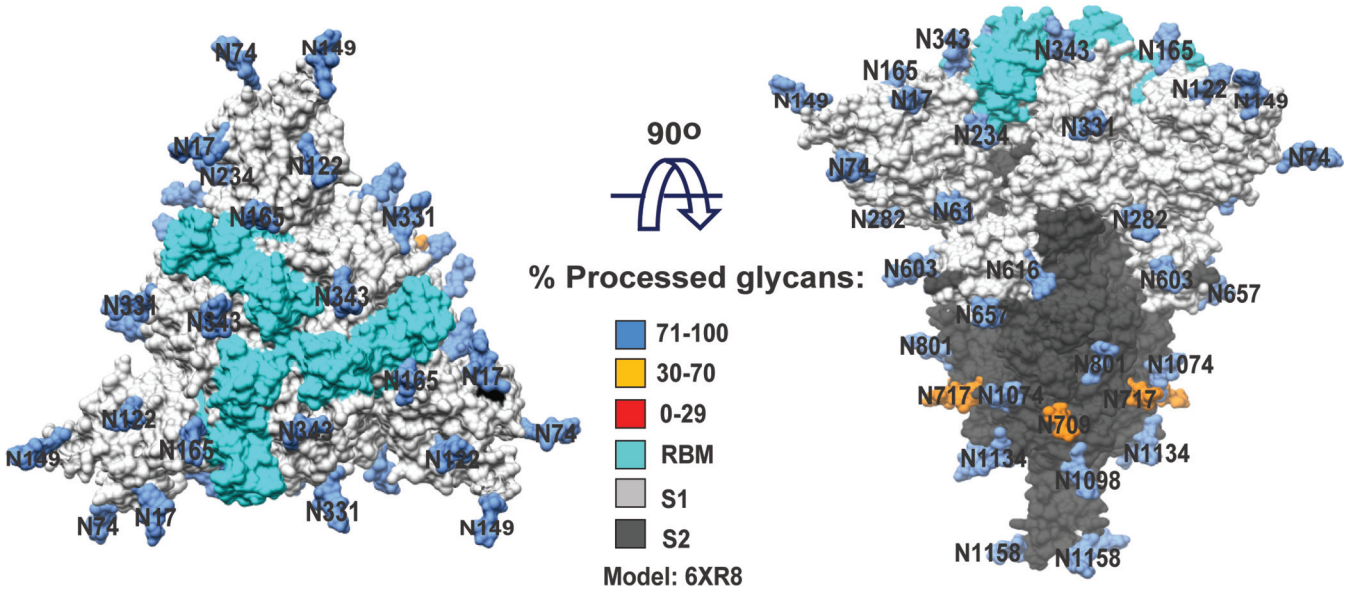


**FIG 11** Location of glycans on the SARS-CoV-2 S glycoprotein trimer. N-linked glycans associated with the indicated asparagine residues are shown on the cryo-EM structure of a solubilized SARS-CoV-2 S glycoprotein trimer (PDB entry 6XR8) (71). The S1 subunits are colored light gray, and the S2 subunits are colored dark gray. The receptor-binding motif is colored cyan. The glycans are colored according to the level of processing observed in our study.

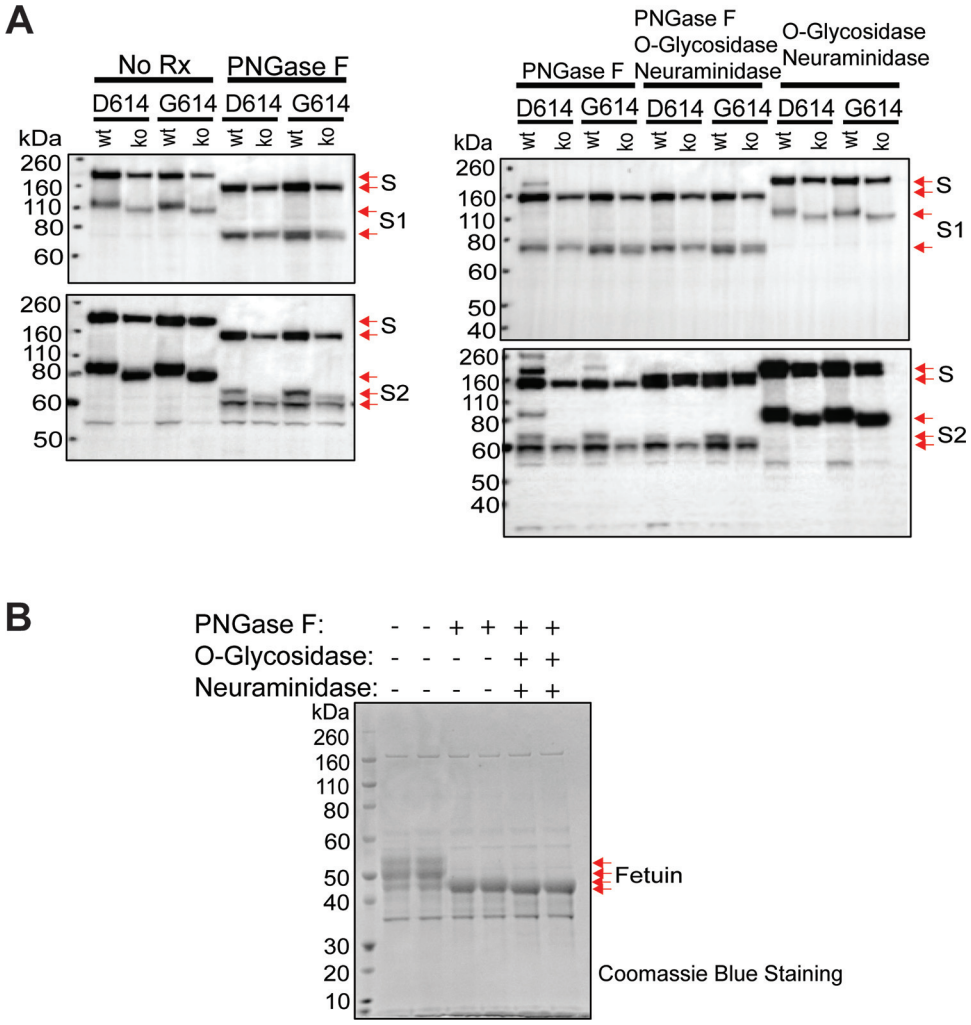


**FIG 12** Characterization of wild-type and D614G S glycoproteins in GALE/GALK2 293T cells. (A) The wild-type SARS-CoV-2 S glycoprotein (D614, with an aspartic acid residue at 614) and the D614G variant (G614, with a glycine residue at 614) were expressed in wild-type 293T cells (wt) or in GALE/GALK2 293T cells (ko) (88). Cell lysates were untreated (No Rx) or were treated with the indicated glycosidase(s), followed by Western blotting with a mouse antibody against S1 (upper) or a rabbit antibody against S2 (lower). The S glycoproteins, either untreated or treated with different glycosidases, are indicated by red arrows. (B) As a control, fetuin, which has N- and O-linked glycans, was treated with the indicated glycosidases. The SDS-polyacrylamide gel was stained with Coomassie blue. The different fetuin glycoforms are indicated by red arrows. The results shown are typical of those obtained in two independent experiments.

wild-type S glycoprotein (Fig. 14). The T323I-pseudotyped viruses infected cells with approximately 41% of the efficiency of viruses pseudotyped with the wild-type S glycoproteins (Fig. 14B), but the infectivity of these viruses decreased further upon freeze-thawing (data not shown). The S673I mutant was processed inefficiently and only supported the infection of pseudotyped VSV vectors at a very low level.

We examined the sensitivity of the two most replication-competent S glycoprotein mutants, T676I and S1170F, to neutralization by sACE2 and sera from convalescing SARS-CoV-2-infected individuals. No significant differences in the neutralization sensitivity of the wild-type and mutant viruses were observed (Fig. 15).

## DISCUSSION

As the extensive glycosylation of the spike (S) glycoprotein can potentially influence SARS-CoV-2 infectivity and sensitivity to antibody inhibition, an understanding of the glycosylation profile of the native S glycoprotein trimer is valuable. Glycosylation of the SARS-CoV-2 S glycoprotein apparently can be influenced by subcellular localization

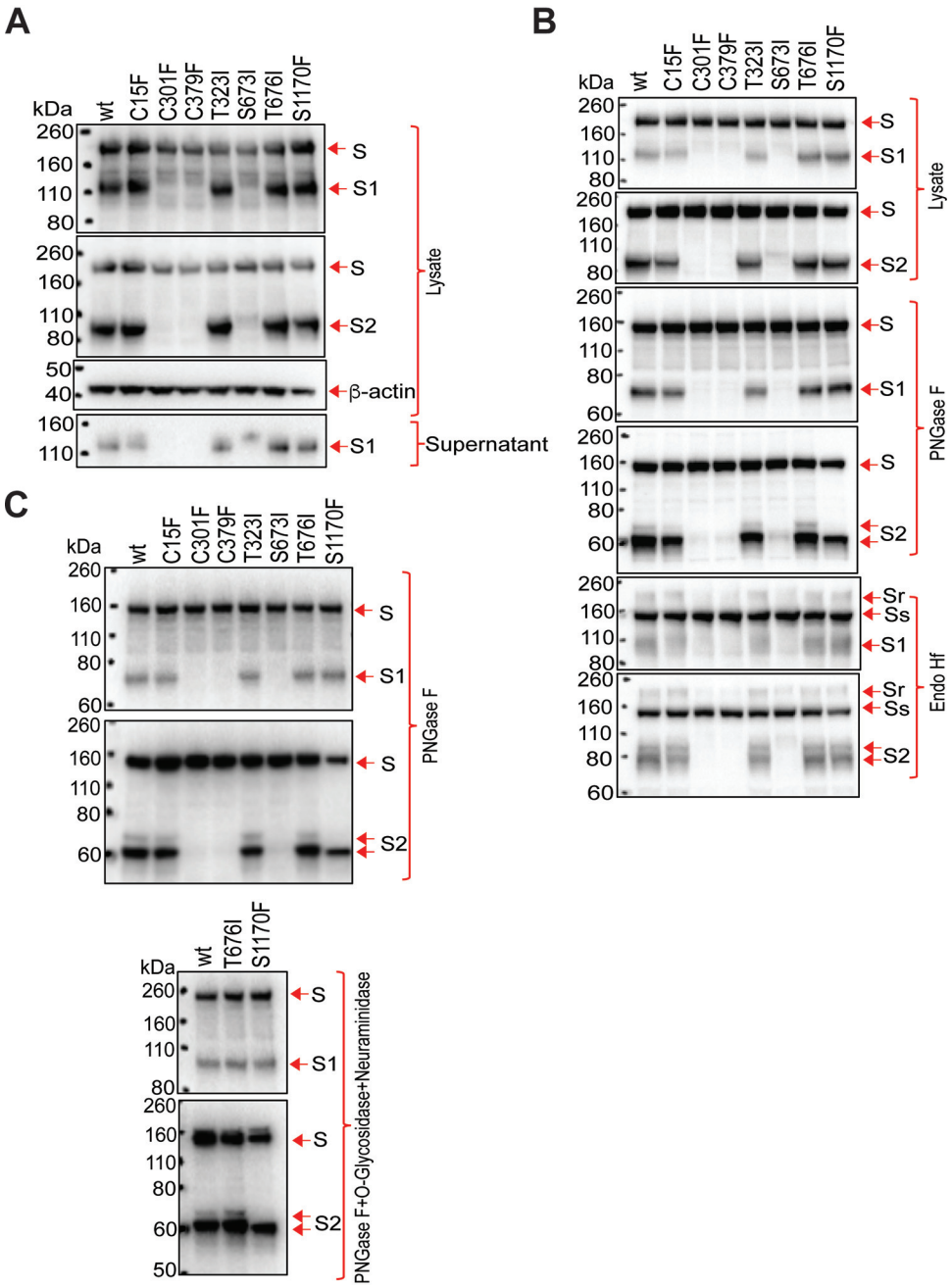


**FIG 13** Phenotypes of natural S glycoprotein variants. (A to C) The wild-type SARS-CoV-2 S glycoprotein and the indicated mutants were expressed in 293T cells. Cell lysates were prepared and, in some cases, treated with PNGase F, Endo Hf, or PNGase F+O-glycosidase plus neuraminidase. The cell lysates were Western blotted. In panel A, cell supernatants were also collected, precleared by centrifugation at 1,800 × *g* for 10 min, and used for precipitation by a 1:100 dilution of NYP01 convalescent-phase serum and protein A-agarose beads. The processing and subunit association indices shown in Table 1 were calculated for each mutant and were normalized to those of the wild-type (wt) S glycoprotein. In panels B and C, the effects of glycosidases on the wild-type and mutant S glycoproteins in cell lysates are shown. Endo Hf-resistant (Sr) and -sensitive (Ss) forms of the uncleaved S glycoprotein are indicated. The results shown are representative of those obtained in four independent experiments.

and the coexpression of viral proteins (52). Because proteolytic activation of the S glycoprotein can occur at the target cell surface or in endosomal compartments during virus entry, the uncleaved S glycoprotein, as well as the cleaved S glycoproteins, on virions can support virus infection (28, 44–46, 94). A SARS-CoV-2 S glycoprotein mutant with an altered site of furin cleavage replicated efficiently in animals but exhibited attenuated pathogenicity (94).

A

| | Disulfide Bond Partner | Location | Processing | Subunit Association | Infectivity (VSVΔG) |
|---|---|---|---|---|---|
| **WT** | NA | NA | ++++ | ++++ | ++++ |
| **C15F** | C136 | Within NTD (S1) | +++ | ++++ | +++ |
| **C301F** | C291 | Within NTD (S1) | - | NA | ++ |
| **C379F** | C432 | Within RBD (S1) | - | NA | ++ |
| **T323I** | NA | NTD-RBD junction | ++++ | ++ | +++ |
| **S673I** | NA | CTD2 of S1 | ++ | ++++ | + |
| **T676I** | NA | CTD2 of S1 | ++++ | +++ | ++++ |
| **S1170F** | NA | HR2 of S2 | +++ | +++ | ++++ |

B

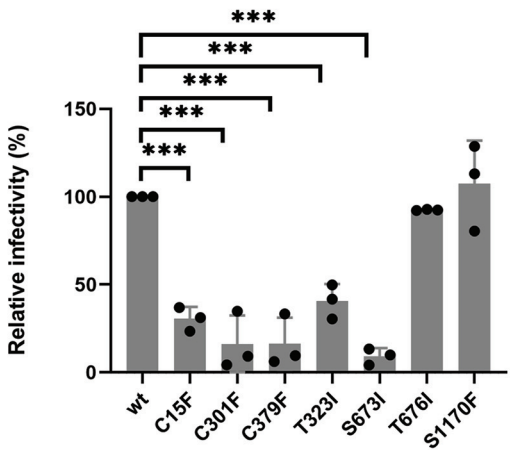


**FIG 14** Phenotypes of natural S glycoprotein variants. (A) The processing, subunit association, and infectivity of the mutant S glycoproteins, relative to those of the wild-type S glycoprotein, are shown (–, undetectable; +, 1 to 10% of wild-type level; ++, 11 to 30% of wild-type level; +++, 31 to 80% of wild-type level; ++++, 81 to 120% of wild-type level; NA, not applicable). The location of the altered amino acid residue in the S glycoprotein is indicated: NTD, N-terminal domain; RBD, receptor-binding domain; CTD2, C-terminal domain 2; HR2, heptad repeat 2. (B) VSV vectors pseudotyped by the indicated SARS-CoV-2 S glycoproteins were used to infect 293T-ACE2 cells. Twenty-four hours later, luciferase activity in the target cells was measured. The infectivity of the mutants is shown relative to that of the wild-type S glycoprotein. The results of three independent experiments are indicated by the black dots, with the means and standard deviations shown in the bar graphs. Statistical analysis was performed using a two-tailed Student's *t* test (***, $P < 0.001$).

Therefore, understanding the glycosylation of the uncleaved and cleaved S glycoproteins is relevant to SARS-CoV-2 biology. The uncleaved S glycoprotein precursor is initially modified in the endoplasmic reticulum by high-mannose carbohydrates; some of these uncleaved/immature S glycoproteins appear on the surface of expressing cells, perhaps by bypassing the Golgi apparatus (28). On SARS-CoV-2 virions, both uncleaved and cleaved S glycoproteins are extensively modified by complex carbohydrates, indicating passage through the Golgi compartment (28, 69, 95). We found that coexpression of the SARS-CoV-2 E protein led to a further enrichment of complex glycans on the uncleaved S glycoprotein on VLPs. These observations provided a rationale for focusing on the S glycoproteins that have been modified during transit through the Golgi compartment. By including a lectin, AAL, that recognizes fucose in the purification scheme, we attempted to increase the representation of S glycoproteins that passed through the Golgi complex, where fucosylation occurs (66–69). This purification strategy allowed an evaluation of the glycan composition of a Golgi-enriched subset of the S glycoproteins synthesized in the expressing cell. We show that the vast majority of the uncleaved and cleaved S glycoproteins on SARS-CoV-2 VLPs can be recognized by AAL, supporting the relevance of the S glycoproteins purified by using this lectin. It is conceivable that forms of the S glycoproteins with lower levels of glycan processing might also be present on virions, depending on host cell types, production levels, and VLP characteristics.

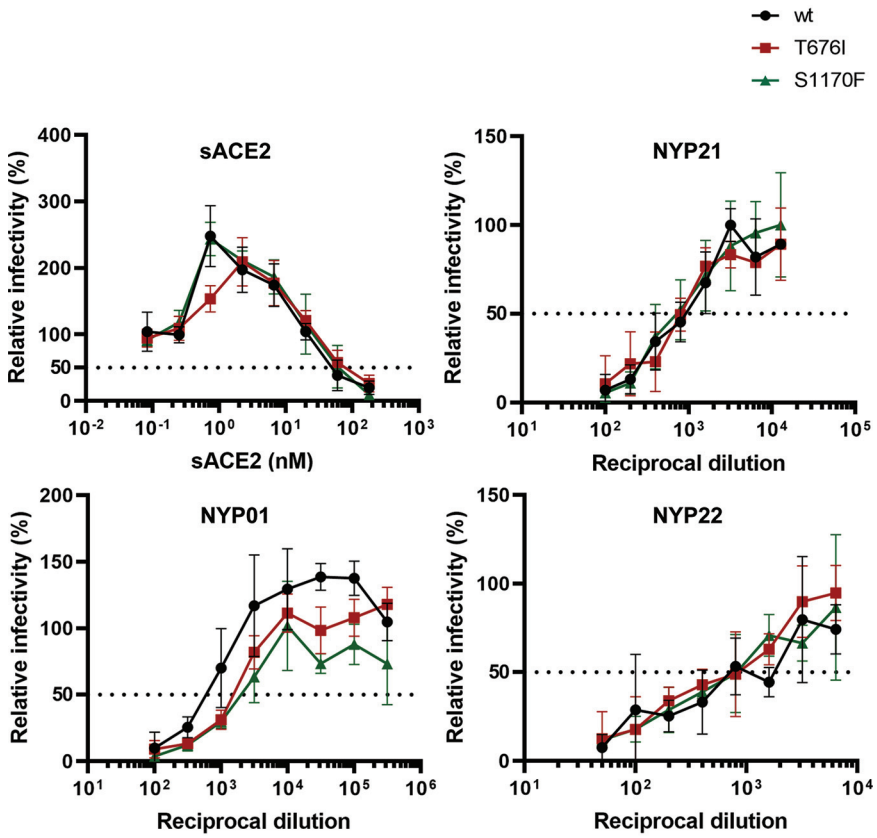


**FIG 15** Neutralization of viruses pseudotyped with S glycoprotein variants. The sensitivity of VSV pseudotypes with the indicated S glycoproteins to neutralization by sACE2 or the NYP01, NYP21, and NYP22 convalescent-phase sera is shown. The infectivity is shown relative to that of a mock-treated virus. The results shown are the means ± standard errors of the means derived from triplicate samples in a single experiment. Similar results were obtained in three independent experiments.

SARS-CoV-2 S glycoproteins produced for use as vaccine immunogens have been designed to allow secretion of soluble trimers, to inhibit furin cleavage, and to stabilize prefusogenic conformations (11, 13, 50, 96–100). The glycosylation profiles of virion S glycoproteins and several of these modified S glycoproteins have been characterized (29, 32, 35, 50–52, 71, 86, 87). Our results agree with the overall predominance of complex carbohydrates of the SARS-CoV-2 S glycoprotein trimer seen in these previous studies. The glycosylation profile of our S glycoprotein preparation most closely resembles that of the S glycoproteins purified from SARS-CoV-2 virions propagated in Vero cells (51). However, compared with these and the other characterized trimers, the wild-type S glycoproteins purified in our study exhibited more glycan processing. Differences among the particular S glycoprotein constructs might account for variation observed in the glycosylation profiles (52). Except for the carboxy-terminal 2×Strep tag, the S glycoprotein that we analyzed is wild type in sequence. Our purified S glycoproteins are trimeric and, in the cleaved fraction, the S1 and S2 subunits maintain their association. The purified trimers preferentially bind MAbs that recognize a closed prefusogenic conformation with all three RBDs in the down position. Nonetheless, we expect that the native, wild-type S glycoprotein trimer is dynamic (70) and might exhibit greater flexibility than S glycoprotein constructs that have been engineered to favor the prefusogenic conformation. This natural S glycoprotein flexibility could increase the access of glycans to processing enzymes in the Golgi apparatus.

We considered the possibility that the uncleaved S glycoproteins in our purified trimer preparation are conformationally heterogeneous and therefore predisposed to complex sugar addition. Functional uncleaved S glycoproteins have been suggested to be more triggerable than cleaved S glycoproteins (28). We observed that the CR3022 MAb, which recognizes open spike conformations with RBDs in the up position (12, 82, 83), binds

only the uncleaved S glycoproteins on the cell surface or in cell lysates (Fig. 4A and B). However, these CR3022-reactive uncleaved S glycoproteins are not modified by complex glycans and, therefore, are not expected to be present in our purified S glycoprotein preparation. The uncleaved S glycoprotein in our purified preparation, like that in VLPs (28), is modified by complex glycans and is not well recognized by the CR3022 MAb (Fig. 4C and D). Future studies will be required to determine whether the cleaved and uncleaved S glycoproteins trafficking through the Golgi compartment acquire different glycan structures.

The source of the S glycoproteins and purification strategy could also influence the glycosylation profile (52). The full-length, wild-type S glycoprotein trimers studied here are distinct from those analyzed by other groups. The inclusion of a fucose-specific lectin in our purification scheme should have increased the representation of S glycoproteins that passed through the Golgi compartment, where complex carbohydrates are added (69). Hypothetically, soluble or virion-associated S glycoproteins passing through the Golgi apparatus might be processed less efficiently than our S glycoproteins, which are anchored in the Golgi membrane. Although Brun et al. (52) also used cells expressing a wild-type, nonstabilized S glycoprotein as their source, they analyzed the glycans only on the S1 glycoprotein monomer that was shed into the cell culture medium. The observed differences in S glycosylation are particularly noteworthy for the Asn 234 glycan, which is predominantly of the high-mannose type in the soluble/modified S glycoproteins, but mostly processed in the wild-type S glycoprotein trimers that we studied. Specific down-selection of the N234 high-mannose glycans by our AAL purification strategy is possible but not likely, given the abundance of multiple fucose-containing glycans on all S glycoforms produced in the 293T-S cells. Asn 234 in the S1 N-terminal domain is near the receptor-binding domain (RBD), and molecular dynamics simulations have suggested that the N234 glycan can modulate the conformational changes that the RBD undergoes in the process of binding ACE2 (101). Moreover, changes in Asn 234 have been reported to affect virus sensitivity to several neutralizing antibodies (102). We note that these phenotypes were revealed by changing Asn 234 to an alanine residue, completely removing the potential N-linked glycosylation site (101, 102). Currently, no experimental evidence exists indicating that the particular type of glycan modifying Asn 234 might influence the binding of ACE2 or neutralizing antibodies directed against nearby epitopes. Another molecular dynamics simulation suggested that the low accessible surface area of oligomannose-type glycans at residues like Asn 234 might limit processing to complex carbohydrates (87). Our results indicate that the N234 glycan on the N-terminal domain is accessible on the unliganded wild-type S glycoprotein trimer for modification to complex carbohydrates. Flexibility in the S glycoprotein N-terminal domain could increase the accessibility and processing of the N234 glycan. The formation of a noncanonical disulfide bond in the N-terminal domain of a subset of our purified S glycoproteins could reflect conformational heterogeneity. Nonetheless, our purified S glycoproteins were precipitated by MAb 4–8, which recognizes an epitope dependent on the tertiary conformation of the N-terminal domain (80). Whether flexibility between the N-terminal domain and RBD could potentially increase the accessibility of the Asn 234 glycan requires further study.

O-linked glycans, which are added in the Golgi compartment (69), were detected on four glycopeptides in the purified S glycoprotein. The occupancy of O-linked glycosylation sites can provide clues to the accessibility of the Ser/Thr residues in the folded S glycoprotein trimer (52). The low occupancy associated with the O-linked glycosylation sites on our purified S glycoprotein is similar to that reported for virion S1 and soluble stabilized S trimers and contrasts with the high O-linked occupancy observed for S1 shed from S-expressing cells or recombinant soluble S1 glycoprotein (52). The low occupancy of the O-linked glycosylation sites is consistent with the antigenicity data (Fig. 4C and D) indicating that the unliganded S glycoproteins that we analyzed largely maintain closed trimer conformations.

We changed three amino acid residues (Thr 323, Thr 676, and Ser 1170) that are potentially O-glycosylated to those amino acid residues found in less common natural SARS-CoV-2 variants. In all three cases, these changes resulted in entry-competent S glycoproteins. However, the infectivity of the T323I mutant was more sensitive to freeze-thawing than that

of viruses pseudotyped with the wild-type S glycoprotein. On the other hand, even though the S1170F change altered posttranslational modification of the S2 glycoprotein, this mutant exhibited wild-type levels of infectivity and resistance to freeze-thawing. Alteration of Thr 676 or Ser 1170 did not significantly change the sensitivity of the pseudotyped viruses to neutralization by sACE2 or convalescent-phase sera.

Of the three naturally observed variants in S glycoprotein cysteine residues, a change in Cys 15 was compatible with an entry-competent S glycoprotein. This implies that the disulfide bond between Cys 15 and Cys 136 within the N-terminal domain is not absolutely required for folding and function of the SARS-CoV-2 S glycoprotein. However, we noted that the infectivity of the C15F mutant virus was compromised after freeze-thawing more than that of the wild-type virus. Apparently, some flexibility in the N-terminal domain can be tolerated in functional S glycoprotein trimers, although the ability of the virus to withstand environmental stress may be affected. Of note, some of the expressed S glycoproteins formed a disulfide bond between Cys 131 and Cys 136 and therefore lacked two of the canonical disulfide bonds (Cys 15-Cys 136 and Cys 131-Cys 166) in the N-terminal domain. Such S conformers, with presumably less stable N-terminal domains, might contribute to viral pathogenesis or to evasion of the host immune response. As discussed above, conformational flexibility in the N-terminal domain could also result in an increase in the accessibility and processing of particular glycans like that on Asn 234.

These studies should assist understanding of the nature and contribution of glycans on the wild-type SARS-CoV-2 S glycoprotein trimer and provide some insight into the impact of natural variation in sites that are glycosylated or disulfide bonded.

## MATERIALS AND METHODS

**Reagents.** Trizma hydrochloride, Trizma base, ammonium bicarbonate, urea, Tris(2-carboxyethyl) phosphine hydrochloride (TCEP), iodoacetamide (IAM), ethanol, 4-vinylpyridine (4-VP), and glacial acetic acid were purchased from Sigma. Other reagents used in this study included optima liquid chromatography (LC)-MS-grade acetonitrile, water, formic acid (Fisher Scientific), sequencing-grade trypsin (Promega), chymotrypsin (Promega), glycerol-free peptidyl-N-glycosidase F (PNGase F) (New England Biolabs), endoglycosidase Hf (Endo Hf) (New England Biolabs), O-glycosidase (New England Biolabs), neuraminidase (New England Biolabs), and fetuin (New England Biolabs). All reagents and buffers were prepared with deionized water purified with a Millipore Direct-Q3 (Billerica, MA) water purification system.

The 2–4, 4–8, and 2–43 monoclonal antibodies (MAbs) were a kind gift from the laboratory of David D. Ho (Columbia University Vagelos College of Physicians and Surgeons) (25, 80, 81). The CR3022 MAb was purchased from Abcam (12, 82, 83).

**Plasmids.** The wild-type and mutant SARS-CoV-2 S glycoproteins were expressed transiently by a pcDNA3.1(−) vector (Thermo Fisher Scientific) (28). The wild-type SARS-CoV-2 spike (S) gene sequence, which encodes an aspartic acid residue at position 614, was obtained from the National Center for Biological Information (NC_045512.20). The gene was modified to encode a $Gly_3$ linker and $His_6$ tag at the carboxyl terminus. The modified S gene was codon optimized, synthesized by Integrated DNA Technologies, and cloned into the pcDNA3.1(−) vector. S mutants were made using Q5 high-fidelity 2× master mix, KLD enzyme mix for site-directed mutagenesis according to the manufacturer's protocol (New England Biolabs), and One-Shot TOP10 competent cells.

Inducible expression of the wild-type SARS-CoV-2 S glycoprotein was achieved using a self-inactivating lentivirus vector comprising TRE3g-SARS-CoV-2-Spike-PSP-StrepII×2.IRES6A.Puro-T2A-GFP (K5650) (28). Here, the codon-optimized *S* gene is under the control of a tetracycline response element (TRE) promoter and encodes the wild-type S glycoprotein with a carboxy-terminal 2×Strep tag. The internal ribosome entry site (IRES6A) allows expression of puro.T2A.EGFP, in which puromycin N-acetyltransferase and enhanced green fluorescent protein (eGFP) are produced by self-cleavage at the Thosea asigna 2A (T2A) sequence.

The plasmid expressing sACE2-Fc was provided by Bing Chen (Boston Children's Hospital) (103); sACE2 was produced as described previously (28). Plasmids expressing the SARS-CoV-2 M, E, and N proteins are described in reference 104.

**Cell lines.** The wild-type SARS-CoV-2 S glycoprotein, with Asp614, was inducibly expressed in Lenti-x-293T human female kidney cells from TaKaRa Bio (catalog number 632180). Lenti-x-293T cells were grown in Dulbecco's modified Eagle's medium (DMEM) with 10% fetal bovine serum (FBS) supplemented with L-glutamine and penicillin-streptomycin (Pen-Strep).

Lenti-x-293T cells constitutively expressing the reverse tetracycline-responsive transcriptional activator (rtTA) (Lenti-x-293T-rtTa cells [D1317]) (28) were used as the parental cells for the 293T-S cell line. The 293T-S (D1483) cells inducibly expressing the wild-type SARS-CoV-2 S glycoprotein with a carboxy-terminal 2×Strep-Tag II sequence (28) were produced by transduction of Lenti-x-293T-rtTA cells with the K5650 recombinant lentivirus vector described above. The packaged K5650 lentivirus vector (60-$\mu$l volume) was incubated with $2 \times 10^5$ Lenti-x-293T-rtTA cells in DMEM, with tumbling at 37°C overnight. The cells were then

transferred to a 6-well plate in 3 ml DMEM–10% FBS–Pen-Strep and subsequently selected with 10 $\mu$g/ml puromycin.

The GALE/GALK2 cells are 293T cells in which the genes encoding UDP-galactose-4-epimerase (GALE) and galactokinase 2 (GALK2) were knocked out by CRISPR/CAS9 technology (88). The GALE/GALK2 cells were obtained from Kerafast (88).

**Expression and processing of S glycoprotein variants.** 293T cells were transfected with plasmids expressing the wild-type and mutant SARS-CoV-2 S glycoproteins. On the day prior to transfection, 293T cells were seeded in 6-well plates at a density of $1 \times 10^6$/well. Cells were transfected with 1 $\mu$g of the S-expressing plasmid, using Lipofectamine 3000 according to the manufacturer's instructions. Two days after transfection, cells were lysed with lysis buffer (1× phosphate-buffered saline [PBS], 1% NP-40, and 1× protease inhibitor cocktail) and the cell lysates analyzed by Western blotting. Samples were Western blotted with 1:2,000 dilutions of either rabbit anti-SARS-Spike S1 or mouse anti-SARS-Spike S1, rabbit anti-SARS-Spike S2 (Sino Biologicals), or a 1:5,000 dilution of mouse anti-$\beta$-actin as the primary antibodies. Horseradish peroxidase (HRP)-conjugated anti-rabbit or anti-mouse antibodies at a dilution of 1:5,000 were used as secondary antibodies in the Western blots. The adjusted integrated volumes of S, S1, and S2 bands from unsaturated Western blots were calculated using Fiji ImageJ. The values for the processing of mutant S glycoproteins were calculated and normalized to the values for the wild-type S glycoprotein (WT) as

$$\text{Processing level} = (\text{S1/S} \times \text{S2/S})_{\text{mutant}} \div (\text{S1/S} \times \text{S2/S})_{\text{WT}}$$

For production of VLPs, the SARS-CoV-2 S glycoprotein was coexpressed with M, E, and N proteins, individually or in combination. One day before transfection, 293T cells were seeded into 10-cm dishes at a density of $5.5 \times 10^6$/dish. The next day, the cells were transfected with 3 $\mu$g of each expressor plasmid or with an empty vector plasmid to keep the total amount of DNA transfected at 12 $\mu$g. Two days after transfection, cell lysates were prepared as described above. Cell supernatants were cleared at 900 × *g* for 15 min, followed by centrifugation at 110,000 × *g* for 1 h at 4°C. Pellets were washed with 800 $\mu$l of 1× PBS and then resuspended in 90 $\mu$l lysis buffer for 5 min on ice. In some cases, cell lysates and pellets prepared from cell supernatants were treated with PNGase F, endoglycosidase Hf (Endo Hf), or O-glycosidase plus neuraminidase (New England Biolabs) according to the manufacturer's instructions. Samples were analyzed by Western blotting as described above.

**S1 shedding from S glycoprotein-expressing cells.** 293T cells were transfected with pcDNA3.1(−) plasmids expressing the wild-type and mutant SARS-CoV-2 S glycoproteins, using Lipofectamine 3000 according to the manufacturer's protocol. Cell supernatants were collected, cleared by centrifugation at 1,800 × *g* for 10 min, and incubated with a 1:100 dilution of NYP01 convalescent-phase serum and protein A-agarose beads for 1 to 2 h at room temperature. Beads were washed three times and samples were Western blotted with a mouse anti-S1 antibody. Band intensity was determined as described above. The subunit association index of each mutant was calculated as

$$\text{Subunit association} = \left(\frac{\text{lysate S1}}{\text{shed S1}}\right)_{\text{mutant}} \div \left(\frac{\text{lysate S1}}{\text{shed S1}}\right)_{\text{WT}}$$

**Recognition of cell surface S glycoproteins by monoclonal antibodies.** For immunoprecipitation of cell surface S glycoproteins, doxycycline-induced 293T-S cells were washed with washing buffer (1× PBS plus 5% FBS). The cells were then incubated with 6 $\mu$g/ml antibody for 1 h at 4°C. After washing three times in washing buffer, the cells were lysed in NP-40 lysis buffer (1% NP-40, 1× PBS, 1× protease inhibitor cocktail) for 5 min on ice. The lysates were cleared by centrifugation at 13,200 × *g* for 10 min at 4°C, and the clarified supernatants were incubated with protein A-agarose beads for 1 h at room temperature. The beads were pelleted (1,000 rpm for 1 min) and washed three times with final wash buffer (1× PBS, 0.5% NP-40). The beads were suspended in lithium dodecyl sulfate (LDS) sample buffer, boiled, and analyzed by Western blotting as described above. In some cases, the precipitated proteins were treated with PNGase F or Endo Hf prior to SDS-PAGE and Western blotting.

For analysis of total glycoprotein expression in the cell, some of the clarified lysates were saved before the addition of protein A-agarose beads and analyzed by Western blotting as described above. These samples are referred to as input.

**AAL recognition of the S glycoproteins on SARS-CoV-2 VLPs.** One day before transfection, $1.8 \times 10^7$ 293T-S cells were seeded in a 15-cm tissue culture dish. The next day, the cells were transfected with 12 $\mu$g of each plasmid expressing the SARS-CoV-2 M, E, and N proteins, using Lipofectamine 3000 (Thermo Fisher Scientific). Following transfection, the cells were incubated in medium containing 1 $\mu$g/ml doxycycline. Two days later, cells were lysed in lysis buffer (1× PBS, 1% Cymal-5, 1× protease inhibitor cocktail). The cell lysates were used to confirm expression of M, E, N, and S proteins.

Cell supernatants were cleared at 900 × *g* for 15 min, followed by centrifugation at 110,000 × *g* for 1 h at 4°C. The pellets were resuspended in 660 $\mu$l lysis buffer. After clearance by centrifugation at 16,100 × *g* for 30 min at 4°C, 60 $\mu$l of the lysate was set aside as the input sample. The remaining lysate was divided into two halves, which were incubated for 1 h at room temperature with 20 $\mu$l of either AAL-agarose resin (number AL-1393-2; Vector Laboratories) or protein A-agarose beads. The suspensions were then applied to Econo-Pac columns (Bio-Rad) with gravity flow. The flowthrough fractions were incubated as above with fresh AAL-agarose resin or protein A-agarose beads, and the process was repeated. The final flowthrough fractions were retained. The columns were washed with 2 ml washing buffer (1× PBS, 0.5% Cymal-5). The beads were resuspended in 300 $\mu$l 1× LDS buffer and, along with the final flowthrough, analyzed by Western blotting for the S glycoproteins.

**Purification of the S glycoproteins.** To express the SARS-CoV-2 S glycoprotein for purification, 293T-S cells were induced with 1 $\mu$g/ml doxycycline for 2 days. The cells were resuspended in 1× PBS and

spun at 4,500 × *g* for 15 min at 4°C. Cell pellets were collected and lysed by incubating in lysis buffer (20 mM Tris HCl [pH 8.0], 150 mM NaCl, 1% Cymal-5, 1× protease inhibitor cocktail [Roche]) on ice for 10 min. Cell lysates were spun at 10,000 × *g* for 20 min at 4°C, and the supernatant was incubated with Strep-Tactin XT superflow resin (IBA number 2-4030-010) by rocking end over end at room temperature for 1.5 h in a 50-ml conical tube. After incubation, the supernatant-resin suspension was applied to a Bio-Rad Econo-Pac column allowing flow-through by gravity, followed by washing with 20 bed volumes of washing buffer (IBA number 2-1003-100, containing 0.5% Cymal-5) and elution with 10 bed volumes of elution buffer (IBA number 2-1042-025, containing 0.5% Cymal-5 and 1× protease inhibitor cocktail). For the second step of purification, the eluate was incubated with AAL-agarose resin (number AL-1393-2; Vector Laboratories) at room temperature for 1 h in a 10-ml conical tube. The eluate-AAL resin suspension was applied to a Bio-Rad Econo-Pac column for gravity flowthrough. The column was washed with 20 bed volumes of washing buffer (20 mM Tris-HCl [pH 8.0], 150 mM NaCl, 0.5% Cymal-5, 1× protease inhibitor cocktail [Roche]), after which the sample was eluted with 10 bed volumes of elution buffer (9 parts elution buffer [Vector Laboratories number ES-3100-100], 0.5 parts 1 M Tris-HCl [pH 8.0], 0.5 parts 10% Cymal-5). The eluate was buffer exchanged by ultrafiltration three times to remove fucose; this was accomplished using a 15-ml ultrafiltration tube (number UFC903024; Thermo Fisher Scientific) at 4,000 × *g* at room temperature with a buffer consisting of 20 mM Tris-HCl (pH 8.0), 150 mM NaCl, and 0.5% Cymal-5.

**Precipitation of the purified S glycoproteins by monoclonal antibodies and sACE2-Fc.** The S glycoproteins, purified as described above, were incubated with monoclonal antibodies (6 $\mu$g/ml) or sACE2-Fc (30 $\mu$g/ml). In some cases, antibody precipitation was carried out in the absence or presence of sACE2 (27 $\mu$g/ml). After incubation with protein A-agarose, the precipitates were analyzed by Western blotting with mouse antibody against S1 and rabbit antibody against S2, as described above.

**Proteolytic digestion of SARS-CoV-2 spike glycoproteins for glycosylation analysis.** The purified SARS-CoV-2 S glycoprotein samples (30 $\mu$g) at a concentration of ~0.03 mg/ml were denatured with 7 M urea in 100 mM Tris buffer (pH 8.5), reduced at room temperature for 1 h with TCEP (5 mM), and alkylated with 20 mM IAM at room temperature for another hour in the dark. The reduced and alkylated samples were buffer exchanged with 50 mM ammonium bicarbonate (pH 8) using a 50-kDa molecular weight cutoff filter (Millipore) prior to protease digestion. The resulting buffer-exchanged sample was aliquoted into two portions, one digested with trypsin and the other with chymotrypsin. All protease digestions were performed according to the manufacturer's suggested protocols. Digestion with trypsin was performed with a 30:1 protein-enzyme ratio at 37°C for 18 h; chymotrypsin digestion was performed with a 20:1 protein-enzyme ratio at 30°C for 10 h; and the combination of both proteases (a mixture of trypsin and chymotrypsin) was performed using the same protein-enzyme ratio as that used for single enzyme digestion and incubated overnight at 37°C. Ten-microliter aliquots from each digest were treated with PNGase F and incubated at 37°C. The digests were either directly analyzed or stored at −20°C until further analysis.

**Chromatography and mass spectrometry.** High-resolution LC-MS experiments were performed using an Orbitrap Fusion Lumos Tribrid (Thermo Scientific) mass spectrometer equipped with an electron transfer dissociation (ETD) option that is coupled to an Acquity UPLC M-Class system (Waters). Mobile phases consisted of solvent A (99.9% deionized $H_2O$ plus 0.1% formic acid) and solvent B (99.9% $CH_3CN$ plus 0.1% formic acid). Three microliters of the sample was injected onto a $C_{18}$ PepMap 300 column (300 $\mu$m inner diameter by 15 cm, 300 Å; Thermo Fisher Scientific) at a flow rate of 3 $\mu$l/min. The following $CH_3CN/H_2O$ multistep gradient was used: 3% B for 3 min, followed a linear increase to 45% B in 50 min and then a linear increase to 90% B in 15 min. The column was held at 90% B for 10 min before reequilibration. All mass spectrometric analyses were performed in the positive ion mode using data-dependent acquisition with the instrument set to run in 3-s cycles for the survey and two consecutive MS/MS scans with collision-induced dissociation (CID) and ETD (either EThcD or ETciD). The full MS survey scans were acquired in the Orbitrap in the mass range 400 to 1,800 *m/z* at a resolution of 120,000 at *m/z* 200 with an automatic gain control target of $4 \times 10^5$. Following a survey scan, MS/MS scans were performed on the most intense ions with charge states ranging from 2 to 8 and with intensity greater than 5,000. CID was carried out at with a collision energy of 30%, while ETD was performed using the calibrated charge-dependent reaction time. Resulting fragments were detected using rapid scan rate in the ion trap.

**Glycopeptide identification and disulfide bond analysis.** Glycopeptide compositional analyses were performed as described previously (105, 106). Briefly, glycopeptide compositions were determined manually from both MS and tandem MS data of a glycopeptide-rich region of the LC/MS data. Glycopeptide peaks from high-resolution MS data in this region were identified from a cluster of peaks whose mass difference corresponds to the masses of monosaccharide units (hexose, HexNAc, NeuAc, and fuc). The compositions for the set of glycopeptides were then determined from fragment mass information from CID and ETD data. This information consists of the Y1 ion for identifying the peptide portion, the glycosidic bond cleavages resulting from the losses of the monosaccharide units from CID data, and the peptide backbone information from ETD data. Once the peptide portion was determined, plausible glycopeptide compositions for the set of peaks for the glycopeptide-rich region were obtained using the high-resolution MS data and GlycoPep DB (107). The putative glycopeptide composition for each glycopeptide-rich region in the LC-MS data was confirmed manually from CID and ETD data. The full list of glycoforms is provided in supplemental material, and the percentage of each type of composition, i.e., high-mannose or processed, is reported here. These percentages are obtained by tallying the relative proportion of high-mannose or processed glycoforms, where each glycoform is weighted equally. The percentages are not meant to correspond to the absolute glycan abundance of high-mannose or processed glycoforms, a quantity that is not precisely knowable, since different glyopeptide glycoforms have different ionization efficiencies (108).

Disulfide bond patterns of SARS CoV-2 spike glycoprotein were determined by mapping the disulfide-linked peptides. Data analysis was performed using the Mascot (v 2.7) search engine (109) for peptides containing free cysteine residues, and disulfide bond patterns were analyzed manually as described previously (110, 111). Briefly, to determine peptides containing free cysteine residues, raw data generated from LC-MS/MS experiments were converted to MGF format using an open-source tool, msConvert. The MGF files were then

searched against the UniProt SARS-CoV-2 database (https://covid-19.uniprot.org/; 106 sequences, 69,061 residues; April 2021) concatenated with a custom database (182 sequences, 110,199 residues) and Swiss-Prot database (2021_02 release, 564,638 sequences, 203,519,613 residues; taxonomy, viruses) using Mascot v. 2.7.0 (MatrixScience). The following search parameters were used: enzyme used, either trypsin alone or combination of trypsin and chymotrypsin, a maximum miscleavage of 2 per peptide, mass tolerance of 10 ppm for precursor and ±0.6 Da for fragment ions. Amino acid modifications were the following: fixed, pyridylethyl (Cys); variable, deamidation (N/Q), Gln→pyro-Glu(N-term Q), and oxidation (M). An automatic decoy search was applied to determine the false discovery rate (FDR) and, when possible, peptides were evaluated at 1% FDR. Mascot ion score cutoffs of 40 and 38 were used for samples digested with trypsin alone and for samples digested with a combination of trypsin and chymotrypsin, respectively. Using these parameters, no peptide was identified with free cysteine, which indicates that the cysteine-containing peptides are all disulfide bonded. To this end, all disulfide-bonded peptides were analyzed manually.

**VSV pseudotyped by S glycoproteins.** VSV was pseudotyped with S glycoproteins expressed stably in 293T-S cells or transiently in 293T cells. 293T-S cells in 6-well plates were induced with 1 $\mu$g/ml doxycycline or, as a control, incubated in standard medium without doxycycline. For transient expression, subconfluent 293T cells in a T75 flask were transfected with 15 $\mu$g of the SARS-CoV-2 S expression plasmid using 60 $\mu$l of 1 mg/ml polyethylenimine (PEI). Twenty-four hours later, cells were infected at a multiplicity of infection of 3 to 5 for 2 h at 37°C with rVSV-ΔG pseudovirus complemented in *trans* with the G glycoprotein and bearing a luciferase gene (Kerafast). Cells were then washed 6 times with DMEM plus 10% FBS and returned to culture. Cell supernatants containing S-pseudotyped VSV were harvested 24 h later, clarified by low-speed centrifugation (900 × *g* for 10 min), and either characterized immediately or stored at −80°C for later analysis.

**Syncytium formation assay.** 293T-S cells in 6-well plates were cotransfected with 1 $\mu$g each of an eGFP-expressing plasmid and a plasmid expressing hACE2 with Lipofectamine 3000 (Thermo Fisher Scientific). Cells were then incubated in either standard (control) medium or medium containing 1 $\mu$g/ml doxycycline. Twenty-four hours after transfection, cells were stained with BioTracker NIR694 nuclear dye (Sigma-Aldrich) and imaged using a fluorescence microscope with green and red filters. In parallel, cell lysates were collected for Western blotting as described above.

**Virus infectivity.** VSV-ΔG vectors pseudotyped with SARS-CoV-2 S glycoprotein variants were produced as described above. The recombinant viruses were incubated with 293T-ACE2 cells, and 24 h later, luciferase activity in the cells was measured.

**Virus neutralization by sACE2 and sera.** Neutralization assays were performed by adding 200 to 300 50% tissue culture infectious doses ($TCID_{50}$) of rVSV-ΔG pseudotyped with SARS-CoV-2 S glycoprotein variants into serial dilutions of sACE2 and sera. The mixture was dispensed onto a 96-well plate in triplicate and incubated for 1 h at 37°C. Approximately $4 \times 10^4$ 293T-ACE2 cells were then added to each well, and the cultures were maintained for an additional 24 h at 37°C before luciferase activity was measured. Neutralization activity was calculated from the reduction in luciferase activity compared to controls using GraphPad Prism 8 (GraphPad Software Inc.).

**Data availability.** The raw MS data have been deposited in the Mass Spectrometry Interactive Virtual Environment (MassIVE) repository, along with search parameters and assignment criteria. MassIVE may be found at https://massive.ucsd.edu/ProteoSAFe/static/massive.jsp. The dataset identifier is MSV000087606, and it can be accessed at ftp://MSV000087606@massive.ucsd.edu. Summaries of the glycopeptide compositions and annotated MS/MS spectra for key novel glycopeptide assignments are available in Table S1 and Fig. S1, respectively.

## ACKNOWLEDGMENTS

We thank Elizabeth Carpelan for preparation of the manuscript. We thank Peihui Wang (Shandong University), Yuan Liu (Cornell University), Lihong Liu and David D. Ho (Columbia University Vagelos College of Physicians and Surgeons), Michael Farzan (Scripps Florida), and Bing Chen (Harvard Medical School) for reagents.

This study was supported by the University of Alabama at Birmingham Center for AIDS Research (NIH P30 AI27767), by grants from the National Institutes of Health (AI125093 to H.D., J.C.K., and J.S. and R35 GM103054 to H.D.), and by funding to J.S. from the late William F. McCarty-Cooper.

S.Z., H. Desaire, and J.S. conceived the study. H. Ding and J.C.K. established the SARS-CoV-2 S glycoprotein-expressing cells. S.Z. and S.A. analyzed the expression and function of S glycoprotein variants. S.Z. purified the SARS-CoV-2 S glycoproteins and characterized the antigenicity of the purified glycoproteins. E.P.G. and H. Desaire analyzed the glycosylation and disulfide bonding of the purified S glycoproteins. S.Z., E.P.G., H. Desaire, and J.S. wrote the manuscript. All authors contributed to data analysis and editing of the manuscript.

## REFERENCES

1. Li Q, Guan X, Wu P, Wang X, Zhou L, Tong Y, Ren R, Leung KSM, Lau EHY, Wong JY, Xing X, Xiang N, Wu Y, Li C, Chen Q, Li D, Liu T, Zhao J, Liu M, Tu W, Chen C, Jin L, Yang R, Wang Q, Zhou S, Wang R, Liu H, Luo Y, Liu Y, Shao G, Li H, Tao Z, Yang Y, Deng Z, Liu B, Ma Z, Zhang Y, Shi G, Lam TTY, Wu JT, Gao GF, Cowling BJ, Yang B, Leung GM, Feng Z. 2020. Early transmission dynamics in Wuhan, China, of novel coronavirus-infected pneumonia. N Engl J Med 382:1199–1207. https://doi.org/10.1056/NEJMoa2001316.
2. Huang C, Wang Y, Li X, Ren L, Zhao J, Hu Y, Zhang L, Fan G, Xu J, Gu X, Cheng Z, Yu T, Xia J, Wei Y, Wu W, Xie X, Yin W, Li H, Liu M, Xiao Y, Gao H, Guo L, Xie J, Wang G, Jiang R, Gao Z, Jin Q, Wang J, Cao B. 2020. Clinical

features of patients infected with 2019 novel coronavirus in Wuhan, China. Lancet 395:497–506. https://doi.org/10.1016/S0140-6736(20)30183-5.
3. Wu F, Zhao S, Yu B, Chen YM, Wang W, Song ZG, Hu Y, Tao ZW, Tian JH, Pei YY, Yuan ML, Zhang YL, Dai FH, Liu Y, Wang QM, Zheng JJ, Xu L, Holmes EC, Zhang YZ. 2020. A new coronavirus associated with human respiratory disease in China. Nature 579:265–269. https://doi.org/10.1038/s41586-020-2008-3.
4. Zhou P, Yang XL, Wang XG, Hu B, Zhang L, Zhang W, Si HR, Zhu Y, Li B, Huang CL, Chen HD, Chen J, Luo Y, Guo H, Jiang RD, Liu MQ, Chen Y, Shen XR, Wang X, Zheng XS, Zhao K, Chen QJ, Deng F, Liu LL, Yan B, Zhan FX, Wang YY, Xiao GF, Shi ZL. 2020. A pneumonia outbreak associated with a new coronavirus of probable bat origin. Nature 579:270–273. https://doi.org/10.1038/s41586-020-2012-7.
5. Coronaviridae Study Group of the International Committee on Taxonomy of Viruses. 2020. The species severe acute respiratory syndrome-related coronavirus: classifying 2019-nCoV and naming it SARS-CoV-2. Nat Microbiol 5:536–544. https://doi.org/10.1038/s41564-020-0695-z.
6. Lv M, Luo X, Estill J, Liu Y, Ren M, Wang J, Wang Q, Zhao S, Wang X, Yang S, Feng X, Li W, Liu E, Zhang X, Wang L, Zhou Q, Meng W, Qi X, Xun Y, Yu X, Chen Y, On Behalf Of The Covid-Evidence and Recommendations Working Group. 2020. Coronavirus disease (COVID-19): a scoping review. Euro Surveill https://doi.org/10.2807/1560-7917.ES.2020.25.15.2000125.
7. Dowd JB, Andriano L, Brazel DM, Rotondi V, Block P, Ding X, Liu Y, Mills MC. 2020. Demographic science aids in understanding the spread and fatality rates of COVID-19. Proc Natl Acad Sci U S A 117:9696–9698. https://doi.org/10.1073/pnas.2004911117.
8. Tortorici MA, Veesler D. 2019. Structural insights into coronavirus entry. Adv Virus Res 105:93–116. https://doi.org/10.1016/bs.aivir.2019.08.002.
9. Ou X, Liu Y, Lei X, Li P, Mi D, Ren L, Guo L, Guo R, Chen T, Hu J, Xiang Z, Mu Z, Chen X, Chen J, Hu K, Jin Q, Wang J, Qian Z. 2020. Characterization of spike glycoprotein of SARS-CoV-2 on virus entry and its immune cross-reactivity with SARS-CoV. Nat Commun 11:1620. https://doi.org/10.1038/s41467-020-15562-9.
10. Li F. 2016. Structure, function, and evolution of coronavirus spike proteins. Annu Rev Virol 3:237–261. https://doi.org/10.1146/annurev-virology-110615-042301.
11. Walls AC, Park YJ, Tortorici MA, Wall A, McGuire AT, Veesler D. 2020. Structure, function, and antigenicity of the SARS-CoV-2 spike glycoprotein. Cell 181:281–292. https://doi.org/10.1016/j.cell.2020.02.058.
12. Yuan M, Wu NC, Zhu X, Lee CD, So RTY, Lv H, Mok CKP, Wilson IA. 2020. A highly conserved cryptic epitope in the receptor binding domains of SARS-CoV-2 and SARS-CoV. Science 368:630–633. https://doi.org/10.1126/science.abb7269.
13. Wrapp D, Wang N, Corbett KS, Goldsmith JA, Hsieh CL, Abiona O, Graham BS, McLellan JS. 2020. Cryo-EM structure of the 2019-nCoV spike in the prefusion conformation. Science 367:1260–1263. https://doi.org/10.1126/science.abb2507.
14. Venkat Kumar G, Jeyanthi V, Ramakrishnan S. 2020. A short review on antibody therapy for COVID-19. New Microbes New Infect 35:100682. https://doi.org/10.1016/j.nmni.2020.100682.
15. Wang C, Li W, Drabek D, Okba NMA, van Haperen R, Osterhaus A, van Kuppeveld FJM, Haagmans BL, Grosveld F, Bosch BJ. 2020. A human monoclonal antibody blocking SARS-CoV-2 infection. Nat Commun 11:2251. https://doi.org/10.1038/s41467-020-16256-y.
16. Callaway E. 2020. The race for coronavirus vaccines: a graphical guide. Nature 580:576–577. https://doi.org/10.1038/d41586-020-01221-y.
17. Billington J, Deschamps I, Erck SC, Gerberding JL, Hanon E, Ivol S, Shiver JW, Spencer JA, Van Hoof J. 2020. Developing vaccines for SARS-CoV-2 and future epidemics and pandemics: applying lessons from past outbreaks. Health Secur 18:241–249. https://doi.org/10.1089/hs.2020.0043.
18. Padron-Regalado E. 2020. Vaccines for SARS-CoV-2: lessons from other coronavirus strains. Infect Dis Ther 9:255–274. https://doi.org/10.1007/s40121-020-00300-x.
19. Gottlieb RL, Nirula A, Chen P, Boscia J, Heller B, Morris J, Huhn G, Cardona J, Mocherla B, Stosor V, Shawa I, Kumar P, Adams AC, Van Naarden J, Custer KL, Durante M, Oakley G, Schade AE, Holzer TR, Ebert PJ, Higgs RE, Kallewaard NL, Sabo J, Patel DR, Klekotka P, Shen L, Skovronsky DM. 2021. Effect of bamlanivimab as monotherapy or in combination with etesevimab on viral load in patients with mild to moderate COVID-19: a randomized clinical trial. JAMA 325:632–644. https://doi.org/10.1001/jama.2021.0202.
20. Quinlan BD, Mou H, Zhang L, Guo YU, He W, Ojha A, Parcells MS, Luo G, Li W, Zhong G, Choe H, Farzan M. 2020. The SARS-CoV-2 receptor-binding domain elicits a potent neutralizing response without antibody-dependent enhancement. bioRxiv https://doi.org/10.1101/2020.04.10.036418.
21. Robbiani DF, Gaebler C, Muecksch F, Lorenzi JCC, Wang Z, Cho A, Agudelo M, Barnes CO, Gazumyan A, Finkin S, Hagglof T, Oliveira TY, Viant C, Hurley A, Hoffmann HH, Millard KG, Kost RG, Cipolla M, Gordon K, Bianchini F, Chen ST, Ramos V, Patel R, Dizon J, Shimeliovich I, Mendoza P, Hartweger H, Nogueira L, Pack M, Horowitz J, Schmidt F, Weisblum Y, Michailidis E, Ashbrook AW, Waltari E, Pak JE, Huey-Tubman KE, Koranda N, Hoffman PR, West AP, Jr, Rice CM, Hatziioannou T, Bjorkman PJ, Bieniasz PD, Caskey M, Nussenzweig MC. 2020. Convergent antibody responses to SARS-CoV-2 in convalescent individuals. Nature 584:437–442. https://doi.org/10.1038/s41586-020-2456-9.
22. Rogers TF, Zhao F, Huang D, Beutler N, Burns A, He WT, Limbo O, Smith C, Song G, Woehl J, Yang L, Abbott RK, Callaghan S, Garcia E, Hurtado J, Parren M, Peng L, Ramirez S, Ricketts J, Ricciardi MJ, Rawlings SA, Wu NC, Yuan M, Smith DM, Nemazee D, Teijaro JR, Voss JE, Wilson IA, Andrabi R, Briney B, Landais E, Sok D, Jardine JG, Burton DR. 2020. Isolation of potent SARS-CoV-2 neutralizing antibodies and protection from disease in a small animal model. Science 369:956–963. https://doi.org/10.1126/science.abc7520.
23. Wec AZ, Wrapp D, Herbert AS, Maurer DP, Haslwanter D, Sakharkar M, Jangra RK, Dieterle ME, Lilov A, Huang D, Tse LV, Johnson NV, Hsieh CL, Wang N, Nett JH, Champney E, Burnina I, Brown M, Lin S, Sinclair M, Johnson C, Pudi S, Bortz R, III, Wirchnianski AS, Laudermilch E, Florez C, Fels JM, O'Brien CM, Graham BS, Nemazee D, Burton DR, Baric RS, Voss JE, Chandran K, Dye JM, McLellan JS, Walker LM. 2020. Broad neutralization of SARS-related viruses by human monoclonal antibodies. Science 369:731–736. https://doi.org/10.1126/science.abc7424.
24. Zost SJ, Gilchuk P, Case JB, Binshtein E, Chen RE, Nkolola JP, Schafer A, Reidy JX, Trivette A, Nargi RS, Sutton RE, Suryadevara N, Martinez DR, Williamson LE, Chen EC, Jones T, Day S, Myers L, Hassan AO, Kafai NM, Winkler ES, Fox JM, Shrihari S, Mueller BK, Meiler J, Chandrashekar A, Mercado NB, Steinhardt JJ, Ren K, Loo YM, Kallewaard NL, McCune BT, Keeler SP, Holtzman MJ, Barouch DH, Gralinski LE, Baric RS, Thackray LB, Diamond MS, Carnahan RH, Crowe JE, Jr. 2020. Potently neutralizing and protective human antibodies against SARS-CoV-2. Nature 584:443–449. https://doi.org/10.1038/s41586-020-2548-6.
25. Liu L, Wang P, Nair MS, Yu J, Rapp M, Wang Q, Luo Y, Chan JF, Sahi V, Figueroa A, Guo XV, Cerutti G, Bimela J, Gorman J, Zhou T, Chen Z, Yuen KY, Kwong PD, Sodroski JG, Yin MT, Sheng Z, Huang Y, Shapiro L, Ho DD. 2020. Potent neutralizing antibodies against multiple epitopes on SARS-CoV-2 spike. Nature 584:450–456. https://doi.org/10.1038/s41586-020-2571-7.
26. Klasse PJ, Moore JP. 2020. Antibodies to SARS-CoV-2 and their potential for therapeutic passive immunization. Elife 9:e57877. https://doi.org/10.7554/eLife.57877.
27. Santopolo S, Riccio A, Santoro MG. 2020. The biogenesis of SARS-CoV-2 spike glycoprotein: multiple targets for host-directed antiviral therapy. Biochem Biophys Res Commun https://doi.org/10.1016/j.bbrc.2020.10.080.
28. Nguyen HT, Zhang S, Wang Q, Anang S, Wang J, Ding H, Kappes JC, Sodroski J. 2021. Spike glycoprotein and host cell determinants of SARS-CoV-2 entry and cytopathic effects. J Virol 95:e02304-20. https://doi.org/10.1128/JVI.02304-20.
29. Watanabe Y, Allen JD, Wrapp D, McLellan JS, Crispin M. 2020. Site-specific glycan analysis of the SARS-CoV-2 spike. Science 369:330–333. https://doi.org/10.1126/science.abb9983.
30. Walls AC, Tortorici MA, Frenz B, Snijder J, Li W, Rey FA, DiMaio F, Bosch BJ, Veesler D. 2016. Glycan shield and epitope masking of a coronavirus spike protein observed by cryo-electron microscopy. Nat Struct Mol Biol 23:899–905. https://doi.org/10.1038/nsmb.3293.
31. Xiong X, Tortorici MA, Snijder J, Yoshioka C, Walls AC, Li W, McGuire AT, Rey FA, Bosch BJ, Veesler D. 2018. Glycan shield and fusion activation of a deltacoronavirus spike glycoprotein fine-tuned for enteric infections. J Virol 92:e01628-17. https://doi.org/10.1128/JVI.01628-17.
32. Zhao P, Praissman JL, Grant OC, Cai Y, Xiao T, Rosenbalm KE, Aoki K, Kellman BP, Bridger R, Barouch DH, Brindley MA, Lewis NE, Tiemeyer M, Chen B, Woods RJ, Wells L. 2020. Virus-receptor interactions of glycosylated SARS-CoV-2 spike and human ACE2 receptor. Cell Host Microbe 28:586–601. https://doi.org/10.1016/j.chom.2020.08.004.
33. Wang D, Baudys J, Bundy JL, Solano M, Keppel T, Barr JR. 2020. Comprehensive analysis of the glycan complement of SARS-CoV-2 spike proteins using signature ions-triggered electron-transfer/higher-energy collisional dissociation (EThcD) mass spectrometry. Anal Chem 92:14730–14739. https://doi.org/10.1021/acs.analchem.0c03301.
34. Shajahan A, Supekar NT, Gleinich AS, Azadi P. 2020. Deducing the N- and O-glycosylation profile of the spike protein of novel coronavirus SARS-CoV-2. Glycobiology 30:981–988. https://doi.org/10.1093/glycob/cwaa042.
35. Sanda M, Morrison L, Goldman R. 2020. N and O glycosylation of the SARS-CoV-2 spike protein. bioRxiv https://doi.org/10.1101/2020.07.05.187344.

36. Lontok E, Corse E, Machamer CE. 2004. Intracellular targeting signals contribute to localization of coronavirus spike proteins near the virus assembly site. J Virol 78:5913–5922. https://doi.org/10.1128/JVI.78.11.5913-5922.2004.
37. McBride CE, Li J, Machamer CE. 2007. The cytoplasmic tail of the severe acute respiratory syndrome coronavirus spike protein contains a novel endoplasmic reticulum retrieval signal that binds COPI and promotes interaction with membrane protein. J Virol 81:2418–2428. https://doi.org/10.1128/JVI.02146-06.
38. Stertz S, Reichelt M, Spiegel M, Kuri T, Martinez-Sobrido L, Garcia-Sastre A, Weber F, Kochs G. 2007. The intracellular sites of early replication and budding of SARS-coronavirus. Virology 361:304–315. https://doi.org/10.1016/j.virol.2006.11.027.
39. Ujike M, Huang C, Shirato K, Makino S, Taguchi F. 2016. The contribution of the cytoplasmic retrieval signal of severe acute respiratory syndrome coronavirus to intracellular accumulation of S proteins and incorporation of S protein into virus-like particles. J Gen Virol 97:1853–1864. https://doi.org/10.1099/jgv.0.000494.
40. Shang J, Ye G, Shi K, Wan Y, Luo C, Aihara H, Geng Q, Auerbach A, Li F. 2020. Structural basis of receptor recognition by SARS-CoV-2. Nature 581:221–224. https://doi.org/10.1038/s41586-020-2179-y.
41. Yan R, Zhang Y, Li Y, Xia L, Guo Y, Zhou Q. 2020. Structural basis for the recognition of SARS-CoV-2 by full-length human ACE2. Science 367:1444–1448. https://doi.org/10.1126/science.abb2762.
42. Hoffmann M, Kleine-Weber H, Schroeder S, Kruger N, Herrler T, Erichsen S, Schiergens TS, Herrler G, Wu NH, Nitsche A, Muller MA, Drosten C, Pohlmann S. 2020. SARS-CoV-2 cell entry depends on ACE2 and TMPRSS2 and is blocked by a clinically proven protease inhibitor. Cell 181:271–280. https://doi.org/10.1016/j.cell.2020.02.052.
43. Xia S, Liu M, Wang C, Xu W, Lan Q, Feng S, Qi F, Bao L, Du L, Liu S, Qin C, Sun F, Shi Z, Zhu Y, Jiang S, Lu L. 2020. Inhibition of SARS-CoV-2 (previously 2019-nCoV) infection by a highly potent pan-coronavirus fusion inhibitor targeting its spike protein that harbors a high capacity to mediate membrane fusion. Cell Res 30:343–355. https://doi.org/10.1038/s41422-020-0305-x.
44. Coutard B, Valle C, de Lamballerie X, Canard B, Seidah NG, Decroly E. 2020. The spike glycoprotein of the new coronavirus 2019-nCoV contains a furin-like cleavage site absent in CoV of the same clade. Antiviral Res 176:104742. https://doi.org/10.1016/j.antiviral.2020.104742.
45. Hoffmann M, Kleine-Weber H, Pohlmann S. 2020. A multibasic cleavage site in the spike protein of SARS-CoV-2 is essential for infection of human lung cells. Mol Cell 78:779–784. https://doi.org/10.1016/j.molcel.2020.04.022.
46. Belouzard S, Chu VC, Whittaker GR. 2009. Activation of the SARS coronavirus spike protein via sequential proteolytic cleavage at two distinct sites. Proc Natl Acad Sci U S A 106:5871–5876. https://doi.org/10.1073/pnas.0809524106.
47. Walls AC, Xiong X, Park YJ, Tortorici MA, Snijder J, Quispe J, Cameroni E, Gopal R, Dai M, Lanzavecchia A, Zambon M, Rey FA, Corti D, Veesler D. 2019. Unexpected receptor functional mimicry elucidates activation of coronavirus fusion. Cell 176:1026–1039. https://doi.org/10.1016/j.cell.2018.12.028.
48. Rossen JW, de Beer R, Godeke GJ, Raamsman MJ, Horzinek MC, Vennema H, Rottier PJ. 1998. The viral spike protein is not involved in the polarized sorting of coronaviruses in epithelial cells. J Virol 72:497–503. https://doi.org/10.1128/JVI.72.1.497-503.1998.
49. Pinto D, Park YJ, Beltramello M, Walls AC, Tortorici MA, Bianchi S, Jaconi S, Culap K, Zatta F, De Marco A, Peter A, Guarino B, Spreafico R, Cameroni E, Case JB, Chen RE, Havenar-Daughton C, Snell G, Telenti A, Virgin HW, Lanzavecchia A, Diamond MS, Fink K, Veesler D, Corti D. 2020. Cross-neutralization of SARS-CoV-2 by a human monoclonal SARS-CoV antibody. Nature 583:290–295. https://doi.org/10.1038/s41586-020-2349-y.
50. Bangaru S, Ozorowski G, Turner HL, Antanasijevic A, Huang D, Wang X, Torres JL, Diedrich JK, Tian JH, Portnoff AD, Patel N, Massare MJ, Yates JR, III, Nemazee D, Paulson JC, Glenn G, Smith G, Ward AB. 2020. Structural analysis of full-length SARS-CoV-2 spike protein from an advanced vaccine candidate. Science 370:1089–1094. https://doi.org/10.1126/science.abe1502.
51. Yao H, Song Y, Chen Y, Wu N, Xu J, Sun C, Zhang J, Weng T, Zhang Z, Wu Z, Cheng L, Shi D, Lu X, Lei J, Crispin M, Shi Y, Li L, Li S. 2020. Molecular architecture of the SARS-CoV-2 virus. Cell 183:730–738. https://doi.org/10.1016/j.cell.2020.09.018.
52. Brun J, Vasiljevic S, Gangadharan B, Hensen M, Chandran AV, Hill ML, Kiappes JL, Dwek RA, Alonzi DS, Struwe WB, Zitzmann N. 2021. Assessing antigen structural integrity through glycosylation analysis of the SARS-CoV-2 viral spike. ACS Cent Sci 7:586–593. https://doi.org/10.1021/acscentsci.1c00058.
53. Go EP, Herschhorn A, Gu C, Castillo-Menendez L, Zhang S, Mao Y, Chen H, Ding H, Wakefield JK, Hua D, Liao HX, Kappes JC, Sodroski J, Desaire H. 2015. Comparative analysis of the glycosylation profiles of membrane-anchored HIV-1 envelope glycoprotein trimers and soluble gp140. J Virol 89:8245–8257. https://doi.org/10.1128/JVI.00628-15.
54. Go EP, Ding H, Zhang S, Ringe RP, Nicely N, Hua D, Steinbock RT, Golabek M, Alin J, Alam SM, Cupo A, Haynes BF, Kappes JC, Moore JP, Sodroski JG, Desaire H. 2017. Glycosylation benchmark profile for HIV-1 envelope glycoprotein production based on eleven Env trimers. J Virol 91:e02428-16. https://doi.org/10.1128/JVI.02428-16.
55. Cao L, Pauthner M, Andrabi R, Rantalainen K, Berndsen Z, Diedrich JK, Menis S, Sok D, Bastidas R, Park SR, Delahunty CM, He L, Guenaga J, Wyatt RT, Schief WR, Ward AB, Yates JR, III, Burton DR, Paulson JC. 2018. Differential processing of HIV envelope glycans on the virus and soluble recombinant trimer. Nat Commun 9:3693. https://doi.org/10.1038/s41467-018-06121-4.
56. Torrents de la Pena A, Rantalainen K, Cottrell CA, Allen JD, van Gils MJ, Torres JL, Crispin M, Sanders RW, Ward AB. 2019. Similarities and differences between native HIV-1 envelope glycoprotein trimers and stabilized soluble trimer mimetics. PLoS Pathog 15:e1007920. https://doi.org/10.1371/journal.ppat.1007920.
57. Struwe WB, Chertova E, Allen JD, Seabright GE, Watanabe Y, Harvey DJ, Medina-Ramirez M, Roser JD, Smith R, Westcott D, Keele BF, Bess JW, Jr, Sanders RW, Lifson JD, Moore JP, Crispin M. 2018. Site-specific glycosylation of virion-derived HIV-1 Env is mimicked by a soluble trimeric immunogen. Cell Rep 24:1958–1966. https://doi.org/10.1016/j.celrep.2018.07.080.
58. Siu YL, Teoh KT, Lo J, Chan CM, Kien F, Escriou N, Tsao SW, Nicholls JM, Altmeyer R, Peiris JS, Bruzzone R, Nal B. 2008. The M, E, and N structural proteins of the severe acute respiratory syndrome coronavirus are required for efficient assembly, trafficking, and release of virus-like particles. J Virol 82:11318–11330. https://doi.org/10.1128/JVI.01052-08.
59. Boson B, Legros V, Zhou B, Siret E, Mathieu C, Cosset FL, Lavillette D, Denolly S. 2020. The SARS-CoV-2 Envelope and Membrane proteins modulate maturation and retention of the Spike protein, allowing assembly of virus-like particles. J Biol Chem https://doi.org/10.1074/jbc.RA120.016175:100111.
60. Long AR, O'Brien CC, Malhotra K, Schwall CT, Albert AD, Watts A, Alder NN. 2013. A detergent-free strategy for the reconstitution of active enzyme complexes from native biological membranes into nanoscale discs. BMC Biotechnol 13:41. https://doi.org/10.1186/1472-6750-13-41.
61. Knowles TJ, Finka R, Smith C, Lin YP, Dafforn T, Overduin M. 2009. Membrane proteins solubilized intact in lipid containing nanoparticles bounded by styrene maleic acid copolymer. J Am Chem Soc 131:7484–7485. https://doi.org/10.1021/ja810046q.
62. Jamshad M, Grimard V, Idini I, Knowles TJ, Dowle MR, Schofield N, Sridhar P, Lin YP, Finka R, Wheatley M, Thomas OR, Palmer RE, Overduin M, Govaerts C, Ruysschaert JM, Edler KJ, Dafforn TR. 2015. Structural analysis of a nanoparticle containing a lipid bilayer used for detergent-free extraction of membrane proteins. Nano Res 8:774–789. https://doi.org/10.1007/s12274-014-0560-6.
63. Lee SC, Knowles TJ, Postis VL, Jamshad M, Parslow RA, Lin YP, Goldman A, Sridhar P, Overduin M, Muench SP, Dafforn TR. 2016. A method for detergent-free isolation of membrane proteins in their local lipid environment. Nat Protoc 11:1149–1162. https://doi.org/10.1038/nprot.2016.070.
64. Orwick MC, Judge PJ, Procek J, Lindholm L, Graziadei A, Engel A, Grobner G, Watts A. 2012. Detergent-free formation and physicochemical characterization of nanosized lipid-polymer complexes: Lipodisq. Angew Chem Int Ed Engl 51:4653–4657. https://doi.org/10.1002/anie.201201355.
65. Morrison KA, Akram A, Mathews A, Khan ZA, Patel JH, Zhou C, Hardy DJ, Moore-Kelly C, Patel R, Odiba V, Knowles TJ, Javed MU, Chmel NP, Dafforn TR, Rothnie AJ. 2016. Membrane protein extraction and purification using styrene-maleic acid (SMA) copolymer: effect of variations in polymer structure. Biochem J 473:4349–4360. https://doi.org/10.1042/BCJ20160723.
66. Wu D, Li J, Struwe WB, Robinson CV. 2019. Probing N-glycoprotein microheterogeneity by lectin affinity purification-mass spectrometry analysis. Chem Sci 10:5146–5155. https://doi.org/10.1039/c9sc00360f.
67. Johansen E, Schilling B, Lerch M, Niles RK, Liu H, Li B, Allen S, Hall SC, Witkowska HE, Regnier FE, Gibson BW, Fisher SJ, Drake PM. 2009. A lectin HPLC method to enrich selectively-glycosylated peptides from complex biological samples. J Vis Exp https://doi.org/10.3791/1398.
68. Iskratsch T, Braun A, Paschinger K, Wilson IB. 2009. Specificity analysis of lectins and antibodies using remodeled glycoproteins. Anal Biochem 386:133–146. https://doi.org/10.1016/j.ab.2008.12.005.
69. Stanley P. 2011. Golgi glycosylation. Cold Spring Harb Perspect Biol 3:a005199. https://doi.org/10.1101/cshperspect.a005199.
70. Lu M, Uchil PD, Li W, Zheng D, Terry DS, Gorman J, Shi W, Zhang B, Zhou T, Ding S, Gasser R, Prevost J, Beaudoin-Bussieres G, Anand SP, Laumaea A, Grover JR, Liu L, Ho DD, Mascola JR, Finzi A, Kwong PD, Blanchard SC, Mothes W. 2020. Real-time conformational dynamics of SARS-CoV-2 spikes

on virus particles. Cell Host Microbe 28:880–891. https://doi.org/10.1016/j.chom.2020.11.001.
71. Cai Y, Zhang J, Xiao T, Peng H, Sterling SM, Walsh RM, Jr, Rawson S, Rits-Volloch S, Chen B. 2020. Distinct conformational states of SARS-CoV-2 spike protein. Science 369:1586–1592. https://doi.org/10.1126/science.abd4251.
72. Benton DJ, Wrobel AG, Xu P, Roustan C, Martin SR, Rosenthal PB, Skehel JJ, Gamblin SJ. 2020. Receptor binding and priming of the spike protein of SARS-CoV-2 for membrane fusion. Nature 588:327–330. https://doi.org/10.1038/s41586-020-2772-0.
73. Henderson R, Edwards RJ, Mansouri K, Janowska K, Stalls V, Gobeil SMC, Kopp M, Li D, Parks R, Hsu AL, Borgnia MJ, Haynes BF, Acharya P. 2020. Controlling the SARS-CoV-2 spike glycoprotein conformation. Nat Struct Mol Biol 27:925–933. https://doi.org/10.1038/s41594-020-0479-4.
74. Hsieh CL, Goldsmith JA, Schaub JM, DiVenere AM, Kuo HC, Javanmardi K, Le KC, Wrapp D, Lee AG, Liu Y, Chou CW, Byrne PO, Hjorth CK, Johnson NV, Ludes-Meyers J, Nguyen AW, Park J, Wang N, Amengor D, Lavinder JJ, Ippolito GC, Maynard JA, Finkelstein IJ, McLellan JS. 2020. Structure-based design of prefusion-stabilized SARS-CoV-2 spikes. Science 369:1501–1505. https://doi.org/10.1126/science.abd0826.
75. Ke Z, Oton J, Qu K, Cortese M, Zila V, McKeane L, Nakane T, Zivanov J, Neufeldt CJ, Cerikan B, Lu JM, Peukes J, Xiong X, Krausslich HG, Scheres SHW, Bartenschlager R, Briggs JAG. 2020. Structures and distributions of SARS-CoV-2 spike proteins on intact virions. Nature 588:498–502. https://doi.org/10.1038/s41586-020-2665-2.
76. Lan J, Ge J, Yu J, Shan S, Zhou H, Fan S, Zhang Q, Shi X, Wang Q, Zhang L, Wang X. 2020. Structure of the SARS-CoV-2 spike receptor-binding domain bound to the ACE2 receptor. Nature 581:215–220. https://doi.org/10.1038/s41586-020-2180-5.
77. McCallum M, Walls AC, Bowen JE, Corti D, Veesler D. 2020. Structure-guided covalent stabilization of coronavirus spike glycoprotein trimers in the closed conformation. Nat Struct Mol Biol 27:942–949. https://doi.org/10.1038/s41594-020-0483-8.
78. Wrobel AG, Benton DJ, Xu P, Roustan C, Martin SR, Rosenthal PB, Skehel JJ, Gamblin SJ. 2020. SARS-CoV-2 and bat RaTG13 spike glycoprotein structures inform on virus evolution and furin-cleavage effects. Nat Struct Mol Biol 27:763–767. https://doi.org/10.1038/s41594-020-0468-7.
79. Zhou T, Tsybovsky Y, Gorman J, Rapp M, Cerutti G, Chuang GY, Katsamba PS, Sampson JM, Schon A, Bimela J, Boyington JC, Nazzari A, Olia AS, Shi W, Sastry M, Stephens T, Stuckey J, Teng IT, Wang P, Wang S, Zhang B, Friesner RA, Ho DD, Mascola JR, Shapiro L, Kwong PD. 2020. Cryo-EM structures of SARS-CoV-2 spike without and with ACE2 reveal a pH-dependent switch to mediate endosomal positioning of receptor-binding domains. Cell Host Microbe 28:867–879. https://doi.org/10.1016/j.chom.2020.11.004.
80. Cerutti G, Guo Y, Zhou T, Gorman J, Lee M, Rapp M, Reddem ER, Yu J, Bahna F, Bimela J, Huang Y, Katsamba PS, Liu L, Nair MS, Rawi R, Olia AS, Wang P, Zhang B, Chuang GY, Ho DD, Sheng Z, Kwong PD, Shapiro L. 2021. Potent SARS-CoV-2 neutralizing antibodies directed against spike N-terminal domain target a single supersite. Cell Host Microbe 29:819–833. https://doi.org/10.1016/j.chom.2021.03.005.
81. Rapp M, Guo Y, Reddem ER, Yu J, Liu L, Wang P, Cerutti G, Katsamba P, Bimela JS, Bahna FA, Mannepalli SM, Zhang B, Kwong PD, Huang Y, Ho DD, Shapiro L, Sheng Z. 2021. Modular basis for potent SARS-CoV-2 neutralization by a prevalent VH1–2-derived antibody class. Cell Rep 35:108950. https://doi.org/10.1016/j.celrep.2021.108950.
82. Yuan M, Liu H, Wu NC, Lee CD, Zhu X, Zhao F, Huang D, Yu W, Hua Y, Tien H, Rogers TF, Landais E, Sok D, Jardine JG, Burton DR, Wilson IA. 2020. Structural basis of a shared antibody response to SARS-CoV-2. Science 369:1119–1123. https://doi.org/10.1126/science.abd2321.
83. Wu NC, Yuan M, Bangaru S, Huang D, Zhu X, Lee CD, Turner HL, Peng L, Yang L, Burton DR, Nemazee D, Ward AB, Wilson IA. 2020. A natural mutation between SARS-CoV-2 and SARS-CoV determines neutralization by a cross-reactive antibody. PLoS Pathog 16:e1009089. https://doi.org/10.1371/journal.ppat.1009089.
84. Mou H, Quinlan BD, Peng H, Liu G, Guo Y, Peng S, Zhang L, Davis-Gardner ME, Gardner MR, Crynen G, DeVaux LB, Voo ZX, Bailey CC, Alpert MD, Rader C, Gack MU, Choe H, Farzan M. 2021. Mutations derived from horseshoe bat ACE2 orthologs enhance ACE2-Fc neutralization of SARS-CoV-2. PLoS Pathog 17:e1009501. https://doi.org/10.1371/journal.ppat.1009501.
85. Zhu Z, Desaire H. 2015. Carbohydrates on proteins: site-specific glycosylation analysis by mass spectrometry. Annu Rev Anal Chem (Palo Alto Calif) 8:463–483. https://doi.org/10.1146/annurev-anchem-071114-040240.
86. Zhang Y, Zhao W, Mao Y, Chen Y, Wang S, Zhong Y, Su T, Gong M, Du D, Lu X, Cheng J, Yang H. 2020. Site-specific N-glycosylation characterization of recombinant SARS-CoV-2 spike proteins. Mol Cell Proteomics https://doi.org/10.1074/mcp.RA120.002295.
87. Allen JD, Chawla H, Samsudin F, Zuzic L, Shivgan AT, Watanabe Y, He WT, Callaghan S, Song G, Yong P, Brouwer PJM, Song Y, Cai Y, Duyvesteyn HME, Malinauskas T, Kint J, Pino P, Wurm MJ, Frank M, Chen B, Stuart DI, Sanders RW, Andrabi R, Burton DR, Li S, Bond PJ, Crispin M. 2021. Site-specific steric control of SARS-CoV-2 spike glycosylation. Biochemistry 60:2153–2169. https://doi.org/10.1021/acs.biochem.1c00279.
88. Termini JM, Silver ZA, Connor B, Antonopoulos A, Haslam SM, Dell A, Desrosiers RC. 2017. HEK293T cell lines defective for O-linked glycosylation. PLoS One 12:e0179949. https://doi.org/10.1371/journal.pone.0179949.
89. Korber B, Fischer WM, Gnanakaran S, Yoon H, Theiler J, Abfalterer W, Hengartner N, Giorgi EE, Bhattacharya T, Foley B, Hastie KM, Parker MD, Partridge DG, Evans CM, Freeman TM, de Silva TI, Sheffield C-GG, McDanal C, Perez LG, Tang H, Moon-Walker A, Whelan SP, LaBranche CC, Saphire EO, Montefiori DC, Sheffield COVID-19 Genomics Group. 2020. Tracking changes in SARS-CoV-2 spike: evidence that D614G increases infectivity of the COVID-19 virus. Cell 182:812–827. https://doi.org/10.1016/j.cell.2020.06.043.
90. Zhang L, Jackson CB, Mou H, Ojha A, Rangarajan ES, Izard T, Farzan M, Choe H. 2020. The D614G mutation in the SARS-CoV-2 spike protein reduces S1 shedding and increases infectivity. bioRxiv https://doi.org/10.1101/2020.06.12.148726.
91. Yurkovetskiy L, Wang X, Pascal KE, Tomkins-Tinch C, Nyalile TP, Wang Y, Baum A, Diehl WE, Dauphin A, Carbone C, Veinotte K, Egri SB, Schaffner SF, Lemieux JE, Munro JB, Rafique A, Barve A, Sabeti PC, Kyratsous CA, Dudkina NV, Shen K, Luban J. 2020. Structural and functional analysis of the D614G SARS-CoV-2 spike protein variant. Cell 183:739–751. https://doi.org/10.1016/j.cell.2020.09.032.
92. Elbe S, Buckland-Merrett G. 2017. Data, disease and diplomacy: GISAID's innovative contribution to global health. Glob Chall 1:33–46. https://doi.org/10.1002/gch2.1018.
93. Shu Y, McCauley J. 2017. GISAID: global initiative on sharing all influenza data–from vision to reality. Euro Surveill 22:30494. https://doi.org/10.2807/1560-7917.ES.2017.22.13.30494.
94. Johnson BA, Xie X, Bailey AL, Kalveram B, Lokugamage KG, Muruato A, Zou J, Zhang X, Juelich T, Smith JK, Zhang L, Bopp N, Schindewolf C, Vu M, Vanderheiden A, Winkler ES, Swetnam D, Plante JA, Aguilar P, Plante KS, Popov V, Lee B, Weaver SC, Suthar MS, Routh AL, Ren P, Ku Z, An Z, Debbink K, Diamond MS, Shi PY, Freiberg AN, Menachery VD. 2021. Loss of furin cleavage site attenuates SARS-CoV-2 pathogenesis. Nature 591:293–299. https://doi.org/10.1038/s41586-021-03237-4.
95. Zhang XY, Guo J, Wan X, Zhou JG, Jin WP, Lu J, Wang WH, Yang AN, Liu DX, Shi ZL, Yuan ZM, Li XG, Meng SL, Duan K, Wang ZJ, Yang XM, Shen S. 2020. Biochemical and antigenic characterization of the structural proteins and their post-translational modifications in purified SARS-CoV-2 virions of an inactivated vaccine candidate. Emerg Microbes Infect 9:2653–2662. https://doi.org/10.1080/22221751.2020.1855945.
96. Corbett KS, Edwards DK, Leist SR, Abiona OM, Boyoglu-Barnum S, Gillespie RA, Himansu S, Schafer A, Ziwawo CT, DiPiazza AT, Dinnon KH, Elbashir SM, Shaw CA, Woods A, Fritch EJ, Martinez DR, Bock KW, Minai M, Nagata BM, Hutchinson GB, Wu K, Henry C, Bahl K, Garcia-Dominguez D, Ma L, Renzi I, Kong WP, Schmidt SD, Wang L, Zhang Y, Phung E, Chang LA, Loomis RJ, Altaras NE, Narayanan E, Metkar M, Presnyak V, Liu C, Louder MK, Shi W, Leung K, Yang ES, West A, Gully KL, Stevens LJ, Wang N, Wrapp D, Doria-Rose NA, Stewart-Jones G, Bennett H, et al. 2020. SARS-CoV-2 mRNA vaccine design enabled by prototype pathogen preparedness. Nature 586:567–571. https://doi.org/10.1038/s41586-020-2622-0.
97. Yu J, Tostanoski LH, Peter L, Mercado NB, McMahan K, Mahrokhian SH, Nkolola JP, Liu J, Li Z, Chandrashekar A, Martinez DR, Loos C, Atyeo C, Fischinger S, Burke JS, Slein MD, Chen Y, Zuiani A, Lelis FJN, Travers M, Habibi S, Pessaint L, Van Ry A, Blade K, Brown R, Cook A, Finneyfrock B, Dodson A, Teow E, Velasco J, Zahn R, Wegmann F, Bondzie EA, Dagotto G, Gebre MS, He X, Jacob-Dolan C, Kirilova M, Kordana N, Lin Z, Maxfield LF, Nampanya F, Nityanandam R, Ventura JD, Wan H, Cai Y, Chen B, Schmidt AG, Wesemann DR, Baric RS, et al. 2020. DNA vaccine protection against SARS-CoV-2 in rhesus macaques. Science 369:806–811. https://doi.org/10.1126/science.abc6284.
98. Corbett KS, Flynn B, Foulds KE, Francica JR, Boyoglu-Barnum S, Werner AP, Flach B, O'Connell S, Bock KW, Minai M, Nagata BM, Andersen H, Martinez DR, Noe AT, Douek N, Donaldson MM, Nji NN, Alvarado GS, Edwards DK, Flebbe DR, Lamb E, Doria-Rose NA, Lin BC, Louder MK, O'Dell S, Schmidt SD, Phung E, Chang LA, Yap C, Todd JM, Pessaint L, Van Ry A, Browne S, Greenhouse J, Putman-Taylor T, Strasbaugh A, Campbell TA, Cook

A, Dodson A, Steingrebe K, Shi W, Zhang Y, Abiona OM, Wang L, Pegu A, Yang ES, Leung K, Zhou T, Teng IT, Widge A, et al. 2020. Evaluation of the mRNA-1273 vaccine against SARS-CoV-2 in nonhuman primates. N Engl J Med 383:1544–1555. https://doi.org/10.1056/NEJMoa2024671.

99. Mercado NB, Zahn R, Wegmann F, Loos C, Chandrashekar A, Yu J, Liu J, Peter L, McMahan K, Tostanoski LH, He X, Martinez DR, Rutten L, Bos R, van Manen D, Vellinga J, Custers J, Langedijk JP, Kwaks T, Bakkers MJG, Zuijdgeest D, Rosendahl Huber SK, Atyeo C, Fischinger S, Burke JS, Feldman J, Hauser BM, Caradonna TM, Bondzie EA, Dagotto G, Gebre MS, Hoffman E, Jacob-Dolan C, Kirilova M, Li Z, Lin Z, Mahrokhian SH, Maxfield LF, Nampanya F, Nityanandam R, Nkolola JP, Patel S, Ventura JD, Verrington K, Wan H, Pessaint L, Van Ry A, Blade K, Strasbaugh A, Cabus M, et al. 2020. Single-shot Ad26 vaccine protects against SARS-CoV-2 in rhesus macaques. Nature 586:583–588. https://doi.org/10.1038/s41586-020-2607-z.
100. Bos R, Rutten L, van der Lubbe JEM, Bakkers MJG, Hardenberg G, Wegmann F, Zuijdgeest D, de Wilde AH, Koornneef A, Verwilligen A, van Manen D, Kwaks T, Vogels R, Dalebout TJ, Myeni SK, Kikkert M, Snijder EJ, Li Z, Barouch DH, Vellinga J, Langedijk JPM, Zahn RC, Custers J, Schuitemaker H. 2020. Ad26 vector-based COVID-19 vaccine encoding a prefusion-stabilized SARS-CoV-2 Spike immunogen induces potent humoral and cellular immune responses. NPJ Vaccines 5:91. https://doi.org/10.1038/s41541-020-00243-x.
101. Casalino L, Gaieb Z, Goldsmith JA, Hjorth CK, Dommer AC, Harbison AM, Fogarty CA, Barros EP, Taylor BC, McLellan JS, Fadda E, Amaro RE. 2020. Beyond shielding: the roles of glycans in the SARS-CoV-2 spike protein. ACS Cent Sci 6:1722–1734. https://doi.org/10.1021/acscentsci.0c01056.
102. Li Q, Wu J, Nie J, Zhang L, Hao H, Liu S, Zhao C, Zhang Q, Liu H, Nie L, Qin H, Wang M, Lu Q, Li X, Sun Q, Liu J, Zhang L, Li X, Huang W, Wang Y. 2020. The impact of mutations in SARS-CoV-2 spike on viral infectivity and antigenicity. Cell 182:1284–1294. https://doi.org/10.1016/j.cell.2020.07.012.
103. Xiao T, Lu J, Zhang J, Johnson RI, McKay LGA, Storm N, Lavine CL, Peng H, Cai Y, Rits-Volloch S, Lu S, Quinlan BD, Farzan M, Seaman MS, Griffiths A, Chen B. 2021. A trimeric human angiotensin-converting enzyme 2 as an anti-SARS-CoV-2 agent. Nat Struct Mol Biol 28:202–209. https://doi.org/10.1038/s41594-020-00549-3.
104. Zhang J, Cruz-Cosme R, Zhuang MW, Liu D, Liu Y, Teng S, Wang PH, Tang Q. 2020. A systemic and molecular study of subcellular localization of SARS-CoV-2 proteins. Signal Transduct Target Ther 5:269. https://doi.org/10.1038/s41392-020-00372-8.
105. Go EP, Irungu J, Zhang Y, Dalpathado DS, Liao HX, Sutherland LL, Alam SM, Haynes BF, Desaire H. 2008. Glycosylation site-specific analysis of HIV envelope proteins (JR-FL and CON-S) reveals major differences in glycosylation site occupancy, glycoform profiles, and antigenic epitopes' accessibility. J Proteome Res 7:1660–1674. https://doi.org/10.1021/pr7006957.
106. Irungu J, Go EP, Zhang Y, Dalpathado DS, Liao HX, Haynes BF, Desaire H. 2008. Comparison of HPLC/ESI-FTICR MS versus MALDI-TOF/TOF MS for glycopeptide analysis of a highly glycosylated HIV envelope glycoprotein. J Am Soc Mass Spectrom 19:1209–1220. https://doi.org/10.1016/j.jasms.2008.05.010.
107. Go EP, Rebecchi KR, Dalpathado DS, Bandu ML, Zhang Y, Desaire H. 2007. GlycoPep DB: a tool for glycopeptide analysis using a "Smart Search." Anal Chem 79:1708–1713. https://doi.org/10.1021/ac061548c.
108. Patabandige MW, Pfeifer LD, Nguyen HT, Desaire H. 2021. Quantitative clinical glycomics strategies: a guide for selecting the best analysis approach. Mass Spectrom Rev https://doi.org/10.1002/mas.21688.
109. Perkins DN, Pappin DJ, Creasy DM, Cottrell JS. 1999. Probability-based protein identification by searching sequence databases using mass spectrometry data. Electrophoresis 20:3551–3567. https://doi.org/10.1002/(SICI)1522-2683(19991201)20:18<3551::AID-ELPS3551>3.0.CO;2-2.
110. Go EP, Zhang Y, Menon S, Desaire H. 2011. Analysis of the disulfide bond arrangement of the HIV-1 envelope protein CON-S gp140 DeltaCFI shows variability in the V1 and V2 regions. J Proteome Res 10:578–591. https://doi.org/10.1021/pr100764a.
111. Go EP, Hua D, Desaire H. 2014. Glycosylation and disulfide bond analysis of transiently and stably expressed clade C HIV-1 gp140 trimers in 293T cells identifies disulfide heterogeneity present in both proteins and differences in O-linked glycosylation. J Proteome Res 13:4012–4027. https://doi.org/10.1021/pr5003643.